

# MoFlow: One-Step Flow Matching for Human Trajectory Forecasting via Implicit Maximum Likelihood Estimation based Distillation

Yuxiang Fu<sup>1,2,\*</sup>, Qi Yan<sup>1,2,\*</sup>, Lele Wang<sup>1</sup>, Ke Li<sup>4</sup>, Renjie Liao<sup>1,2,3</sup>

<sup>1</sup>University of British Columbia, <sup>2</sup>Vector Institute for AI,

<sup>3</sup>Canada CIFAR AI Chair, <sup>4</sup>Simon Fraser University

{yuxiang.fu, qi.yan, lelewang}@ece.ubc.ca, keli@sfu.ca, rjliao@ece.ubc.ca

## Abstract

In this paper, we address the problem of human trajectory forecasting, which aims to predict the inherently multi-modal future movements of humans based on their past trajectories and other contextual cues. We propose a novel motion prediction conditional flow matching model, termed MoFlow, to predict  $K$ -shot future trajectories for all agents in a given scene. We design a novel flow matching loss function that not only ensures at least one of the  $K$  sets of future trajectories is accurate but also encourages all  $K$  sets of future trajectories to be diverse and plausible. Furthermore, by leveraging the implicit maximum likelihood estimation (IMLE), we propose a novel distillation method for flow models that only requires samples from the teacher model. Extensive experiments on the real-world datasets, including SportVU NBA games, ETH-UCY, and SDD, demonstrate that both our teacher flow model and the IMLE-distilled student model achieve state-of-the-art performance. These models can generate diverse trajectories that are physically and socially plausible. Moreover, our one-step student model is **100** times faster than the teacher flow model during sampling. The code, model, and data are available at our project page: <https://moflow-imle.github.io/>.

## 1. Introduction

Human trajectory forecasting comprises a dual-purpose mission: 1) to predict future trajectories of human with unparalleled precision and 2) to generate diverse future movements that reflect the uncertainty of the complex decision-making processes inherent to human behaviour. Pedestrian trajectory prediction task plays an important role in modern autonomous driving systems [13, 23, 41, 48], autonomous drones [14] and human-robot interactions [84]. In a multi-agent scene, trajectory forecasting involves predicting the distribution of future paths through the exploitation of individual historic trajectories and mutual influence among agents. Despite significant advancements in recent years [6, 18, 29, 37, 73, 76], predicting future human trajec-

\*Equal Contribution

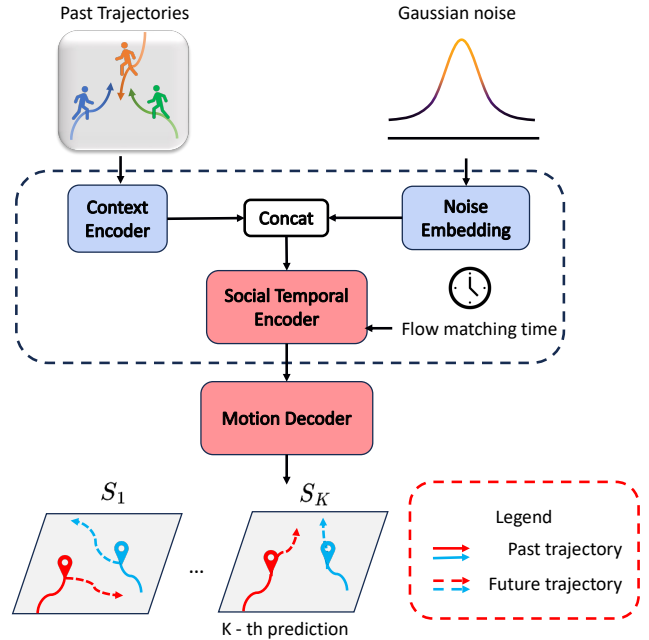


Figure 1. Overview of our MoFlow model, which consists of a social temporal encoder for contextual cues and a motion decoder that predicts  $K$ -shot future trajectories of all agents in a scene.

ories remains a challenging task due to the intrinsic multi-modality of human motion.

To tackle this challenge, the majority of previous studies have turned to generative models [10, 29, 73, 76], capturing the multi-modal nature of potential future paths via a latent variable. Recent works have leveraged the denoising diffusion models (DMs) [18, 28, 45] for probabilistic time series forecasting through their integration with sequence-to-sequence models, due to its outstanding capacity to represent the data distribution. Note that DMs can be seen as special cases of flow-based models with conditional Gaussian probability path [2, 27, 34, 35]. Therefore, we use the term DMs and flow models interchangeably unless specified otherwise. Motion Indeterminacy Diffusion (MID) [18] marks a significant milestone by first applying DMs to human trajectory prediction, where future positions are considered as particles in thermodynamics. Nonetheless, such diffusion based approach encounters several critical drawbacks. First,

for each agent, multiple future trajectories from DMs are sampled independently. As a result, it is common for multiple sampled trajectories to overlap, leading to a lack of spatial diversity. This is particularly unsatisfactory when modeling human trajectories, where the inherent multi-modality suggests that future trajectories should often diverge toward different directions and regions. Second, the sampling process of DMs is notoriously slow and inherently sequential. DMs require a large number of neural function evaluations (NFEs) [61] to numerically integrate a differential equation. This limits their applicability to time-critical tasks, such as autonomous driving, and may compromise safety.

In this paper, we aim to address the above challenges with DMs for human trajectory prediction. The main contributions are outlined as follows:

- We present a novel **Motion prediction Flow** matching (MoFlow) model for trajectory prediction tasks. For each agent in a scene, instead of modeling a single future trajectory, we model multiple future trajectories jointly using the flow model. We design a new flow matching loss in tandem that promotes the learning of a diverse set of future trajectories that well capture the multi-modality of human trajectories.
- We propose a distillation method for flow models based on Implicit Maximum Likelihood Estimation (IMLE) [31]. Compared to existing distillation methods like consistency distillation (CD) [61], it only requires samples from the teacher model, thus being efficient.
- Both MoFlow and the proposed distillation method attain state-of-the-art performance in various metrics on the three human motion datasets, effectively balancing the trade-off between the accuracy and diversity in trajectory forecasting. Our results have the implications as i) our approach accelerates the standard conditional flow matching inference by a great margin, and ii) our IMLE model distills the teacher model in a principled manner that models prediction uncertainty in a sensible way.

## 2. Related work

### 2.1. Human Trajectory Prediction

Human motion trajectories are inherently uncertain [18, 67], as individuals alter their future motion at will or adjust their direction in response to their surroundings. With a historical record of observed trajectories, numerous viable paths emerge for how pedestrians might move forward. In pursuit of modeling the indeterminacy of human trajectory, recent efforts address the dynamic trajectory prediction problem by using an ensemble of deep generative models. For instance, Generative Adversarial Network (GAN) frameworks [10, 19, 54] are adapted to generate future stochastic trajectories. Previous works [29, 73, 76] exploit the conditional variational autoencoder (CVAE) to learn

distributions via variational inference, while CF-VAE [9] adopts conditional normalizing flow to learn a representative prior. More recently, DMs have been introduced for human trajectory forecasting tasks, exhibiting remarkable performance and capturing future multi-modality [18, 45].

### 2.2. Distillation of Diffusion and Flow Models

Denoising DMs [21, 57, 59] and their extended family of flow-matching methods [2, 34, 35] represent an innovative class of deep generative models inspired by non-equilibrium thermodynamics. The concept behind DMs involves gradually corrupting the data with noise through a forward diffusion process and employing a learned reverse process to reconstruct the original data structure. These models have attracted substantial attention for their state-of-the-art performance across a wide array of generative tasks, such as 3D objects [68, 70, 83], video [7, 22, 46, 51] and discrete structure graphs [1, 16, 78]. However, these models suffer from hundreds and thousands of iterative denoising steps required during inference. To accelerate the inference process, many previous works [39, 58, 69] concentrate on developing faster numerical solvers. Notice that sampling process in DMs fundamentally involves solving ordinary differential equations (ODEs) or stochastic differential equations (SDEs) [60], albeit, these approaches still require more than 10 sampling steps to account for discretization error. Distillation of diffusion and flow models emerges with the goal to substitute all the sampling steps with one NFE. In particular, it utilizes a student model to distill the multi-step outputs from the teacher DM [8, 17, 47, 61, 63, 85]. Diffusion distillation [42] incorporates two primary classes:

(1) *Sampling trajectory dynamics refinement.* Prior works often train a student model to approximate the deterministic process of teacher DM during inference. For instance, knowledge distillation [20, 40] trains a student model to transform noise to data. Progressive distillation (PD) [47, 63] involves training a sequence of student models w.r.t the original DM, each requiring half the sampling steps of its predecessor. Rectified flow [25, 35, 36] simulates denoising ODEs to create synthetic datasets while the ReFlow operation enforces a nearly straight flow to the target distribution. Moreover, CD [61] and TRACT [8] train a student model to align its output at one timestep with its output at another timestep along the probability ODE flow, ensuring consistency across multiple timesteps and thus consistent with the teacher. Shortcut models [15] unify self-consistency and flow-matching objectives by incorporating both the current noise level and step size, enabling end-to-end training. This distillation technique accelerates convergence by dividing the process into  $\log_2(T)$  stages, where the step size is progressively increased, effectively reducing the required bootstrap paths.

(2) *Distribution alignment.* The student model distills

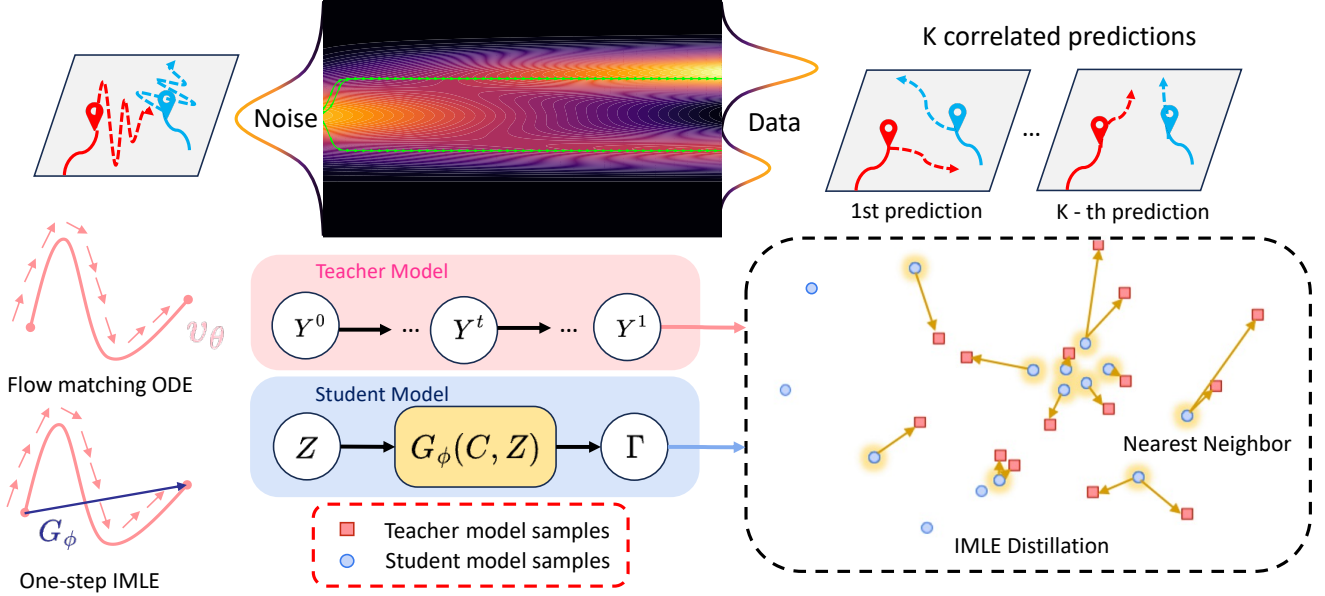


Figure 2. The overall scheme of our proposed MoFlow model and the IMLE distillation framework. **Top:** Solid lines mean past trajectories; dotted lines show multi-modal future predictions. The teacher MoFlow model predicts by solving the denoising ODE, with the green paths being ODE solutions mapping samples from noise to data. **Bottom:** The IMLE objective trains a student model for one-step inference by minimizing the distance between a teacher model sample and its closest counterpart from the student model, as indicated by the arrows.

knowledge by matching its output distribution with that of the teacher diffusion model, leveraging adversarial [55] and distribution-matching [80] objectives. Denoising Diffusion GAN [71] uses GANs for expressive denoising, while Adversarial Distillation Diffusion [55] extends this to the SD-XL Turbo model for efficient image generation. Our method falls into this category. Comparing with other maximum likelihood-based approach like EM distillation [72], our approach does not incorporate expensive MCMC procedures. There is another array of methods that minimize different divergence measures through variational score distillation [65], including reverse KL divergence [79, 80], forward KL divergence [43, 72], and fisher divergence [86].

Regarding accelerating a DM that generates human motion trajectory, LEapfrog Diffusion (LED) [45] designs a deterministic initializer to predict trajectories corresponding to the latent diffusion state at diffusion time step  $\tau$  where  $\tau \ll T$  and  $T$  is the total diffusion time steps. Although this distillation approach enables fast inference, it is often associated with a discernible deterioration in sample quality.

### 3. Background

#### 3.1. Motion Prediction

The goal of motion prediction is to generate plausible future trajectories for agents of interest based on their motion history and that of surrounding agents. Let  $\mathbf{x} = [x_{-T_p+1}, x_{-T_p+2}, \dots, x_0] \in \mathbb{R}^{2T_p}$  represent the observed past movements over  $T_p$  timestamps, where  $x_\tau \in \mathbb{R}^2$  captures the spatial coordinates at time  $\tau$  from a bird’s-eye

view. Given  $A$  agents in the scene, their past trajectories are represented by  $X = [\mathbf{x}_1^\top; \mathbf{x}_2^\top; \dots; \mathbf{x}_A^\top] \in \mathbb{R}^{A \times 2T_p}$ , where  $\mathbf{x}_i$  denotes the past trajectory of the  $i$ -th agent and  $[\cdot; \cdot]$  means stacking row vectors. For simplicity, we use  $C \in \mathbb{R}^{A \times C_a T_p}$  to represent all the contextual information, where  $C_a$  is the number of features per timestamp (e.g., absolute coordinates, relative coordinates with respect to the last frame, and velocity). Let  $\mathbf{y}_i = [y_{i1}, y_{i2}, \dots, y_{iT_f}] \in \mathbb{R}^{2T_f}$  be the ground-truth future trajectory of the  $i$ -th agent across the future  $T_f$  frames, where  $y_{i\tau} \in \mathbb{R}^2$  is the coordinate at future time  $\tau$ . We denote the future trajectories of  $A$  agents in the scene as  $Y = [\mathbf{y}_1^\top; \mathbf{y}_2^\top; \dots; \mathbf{y}_A^\top] \in \mathbb{R}^{A \times 2T_f}$ . In principle, the objective of motion prediction is to train a probabilistic model  $p_\phi(Y|C)$  with parameters  $\phi$ , which captures the multi-modality and the uncertainty of multi-agent motion dynamics. Typically, this model is trained via the maximum likelihood objective  $\max_\phi \mathbb{E}_{(Y,C) \sim p_D} [\log p_\phi(Y|C)]$ , where  $p_D$  stands for the data distribution consisting of the coupled context information and future motion trajectories.

#### 3.2. Flow Matching and Diffusion

Recent advancements in generative models, including flow-matching models [2, 34, 35] and DMs [21, 57, 58, 60], rely heavily on the effective learning of ODEs or SDEs to transform noise into data. While differing in specific formulations, diffusion and flow models share similar generative modeling principles [2, 34]. In this paper, we adopt the simple linear flow objective used in previous works [2, 34, 35]. Given the observed future scene-level trajectories of  $Y^1 \sim q(\cdot)$ , we can linearly interpolate between  $Y^1 \in \mathbb{R}^{A \times 2T_f}$  and

a noise variable with the same dimension,  $Y^0 \sim \mathcal{N}(\mathbf{0}, \mathbf{I})$ , to obtain  $Y^t$ , where the superscript  $t \in [0, 1)$  denotes the time in flow models, rather than the time in motion prediction. In particular, we have,

$$Y^t = (1 - t)Y^0 + tY^1, \quad (3.1)$$

$$U^t = Y^1 - Y^0, \quad (3.2)$$

where the velocity field  $U^t$  induces a probability path that interpolates from the noise distribution to the data distribution. Although  $U^t$  is a function of flow time  $t$  in general, linear flow has a simple constant velocity. During training, we sample  $Y^0$  and  $Y^1$  from a fixed prior distribution and the data distribution, respectively, making the target vector field  $U^t$  fully determined [34]. We train a neural network  $v_\theta$  to approximate the target  $U^t$  by minimizing:

$$\mathcal{L}_{\text{FM}} := \mathbb{E}_{Y^t, Y^1, t} [\|v_\theta(Y^t, C, t) - U^t\|_2^2]. \quad (3.3)$$

Here the learned velocity field  $v_\theta$  also depends on the contextual information  $C$  in the context of motion prediction. To generate samples from a flow model, we first sample noise  $Y^0$  from the standard normal distribution and then iteratively update it towards  $t = 1$  according to the learned velocity field, *i.e.*,  $Y^{t+1} = Y^t + v_\theta(Y^t, C, t)$ , which essentially solves the underlying ODE using the Euler’s method.

## 4. Method

We first present our method for encoding context information, then introduce our flow-based teacher model for motion prediction, and finally describe how to use IMLE to distill this teacher model into a student model for one-step sampling. In Fig. 2, the teacher model is shown at the top, and the distillation process is illustrated at the bottom.

### 4.1. Context Encoding

We start by developing an attention-based context encoder to capture the physical dynamics of agents’ past motion. Recall that  $C \in \mathbb{R}^{A \times C_a T_p}$  denotes the historical state information for all  $A$  agents. To initialize per-agent features, we apply an MLP layer, followed by a transformer encoder module to process inter-agent dynamics:

$$H_0 = \text{MLP}(C),$$

$$H'_0 = H_0 + \text{PE}_A,$$

$$H_{\text{enc}} = \text{MHSA}(Q = H'_0, K = H'_0, V = H'_0),$$

where  $\text{PE}_A$  represents the learnable positional encoding based on agent-specific characteristics, such as differentiating between players and the ball in the NBA sports dataset. Here  $H_0 \in \mathbb{R}^{A \times d}$ . We use the standard multi-head self-attention module in Transformers [64],  $\text{MHSA}(\cdot, \cdot, \cdot)$ , to model interactions between agents within each scene. The context encoder ultimately outputs agent features as  $H_{\text{enc}} \in \mathbb{R}^{A \times d}$ , which are then passed to the motion decoder network, as illustrated by Fig. 1. The architectural detail of

both the spatio-temporal encoder and motion decoder can be found in Appendix A.4.

### 4.2. Flow Matching for Motion Prediction

**Multi-modal Learning Objective.** Ensuring diverse motion patterns is essential for the success of trajectory forecasting models. Previously, motion generative models have been used to draw a flexible number of  $K$  i.i.d. trajectory samples from a given context  $C$ , resulting in multi-modal predictions  $\{Y_1, Y_2, \dots, Y_K\}^1$  as demonstrated in [18, 24]. However, their performance is empirically limited [45], as the i.i.d. predicted trajectories fundamentally cannot account for coherence and consistency among  $K$  predictions, such as reducing self-collision and ensuring diverse mode coverage. Although some deterministic methods can generate correlated  $K$  predictions, research on denoising generative models capable of producing correlated  $K$  ensemble predictions remains limited. To address this issue, we propose using a single flow-matching model with an efficient closest-prediction objective to promote the multi-modality, eliminating the need for extra models or additional training. In contrast, LED [45] has to train an additional initializer to match comparable predictive performance.

By rearranging the linear flow training objective in Eq. (3.3) in the data prediction space, we introduce a neural network  $D_\theta$  and define the equivalent loss:

$$D_\theta(Y^t, C, t) := Y^t + (1 - t)v_\theta(Y^t, C, t), \quad (4.1)$$

$$\mathcal{L}_{\text{FM}} = \mathbb{E}_{Y^t, Y^1, t} \left[ \frac{\|D_\theta(Y^t, C, t) - Y^1\|_2^2}{(1 - t)^2} \right]. \quad (4.2)$$

Please refer to the supplement for the derivation details. This formulation allows  $D_\theta$  to match the future trajectory  $Y^1$  in the data space. Namely,  $D_\theta$  carries out one-step data prediction given noisy vector  $Y^t$  and context  $C$  at time  $t$ . It can be reparameterized to obtain  $v_\theta$  for ODE sampling.

Next, we design a novel loss to train the model  $D_\theta$  as well as promoting the multi-modality. Note that the output dimensionality of  $D_\theta$  in Eq. (4.2) still reflects a single prediction. We first apply a standard Transformer structure (as shown in Fig. 1) to generate  $K$  correlated predictions, where  $D_\theta$  outputs  $K$  scene-level waypoint predictions, denoted by  $\{S_i\}_{i=1}^K$ ,  $S_i \in \mathbb{R}^{A \times 2T_f}$ , alongside corresponding classification logits  $\{\zeta_i\}_{i=1}^K$ ,  $\zeta_i \in \mathbb{R}$ . For simplicity, we omit the time-dependent coefficient in Eq. (4.2) and apply a combined regression and classification loss as follows:

$$\tilde{\mathcal{L}}_{\text{FM}} = \mathbb{E}_{Y^t, Y^1, t} [\|S_{j^*} - Y^1\|_2^2 + \text{CE}(\zeta_{1:K}, j^*)], \quad (4.3)$$

$$j^* = \arg \min_j \|S_j - Y^1\|_2^2, \quad (4.4)$$

where  $\text{CE}(\cdot, \cdot)$  denotes the cross-entropy loss.

<sup>1</sup>We use the superscript  $t$  to indicate time in flow models and the subscript  $k$  to denote the  $k$ -th predicted future.

---

**Algorithm 1** Distilling MoFlow with IMLE

---

- 1: **Require:** Dataset  $p_{\mathcal{D}}$ , IMLE sampling size  $m$ , learning rate  $\eta$ , teacher flow model  $v_{\theta}$
  - 2: Initialize the parameters  $\phi$  of the network  $G_{\phi}$ .
  - 3: **repeat**
  - 4:    $(\cdot, C) \sim p_{\mathcal{D}}$  ▷ Sample context data
  - 5:    $Y_1^0, \dots, Y_K^0 \sim \mathcal{N}(\mathbf{0}, \mathbf{I})$
  - 6:   Solve the ODE via  $v_{\theta}$  to obtain  $\hat{Y}_{1:K}^1$
  - 7:    $Z_1, \dots, Z_m \sim \mathcal{N}(\mathbf{0}, \mathbf{I})$
  - 8:    $\Gamma_j \leftarrow G_{\phi}(C, Z_j), j \in [m]$
  - 9:    $\pi \leftarrow \arg \min_j \mathcal{L}_{\text{IMLE}}(\hat{Y}_{1:K}^1, \Gamma_j)$
  - 10:    $\phi \leftarrow \phi - \eta \nabla_{\phi} \mathcal{L}_{\text{IMLE}}(\hat{Y}_{1:K}^1, \Gamma_{\pi})$
  - 11: **until** converged
- 

**Input-Output Dimension Adaptation.** Now, our flow model handles  $K$ -shot trajectory predictions. Its input includes  $K$  sets of scene-level noisy trajectories,  $Y_{1:K}^t$ . Note that  $Y_i^1$  represents the  $i$ -th possible configuration of future trajectories of all agents in the scene, whereas  $Y_i^t$  represents the corresponding noisy version at flow time  $t$ . To solve the denoising ODEs during sampling, we use the  $K$ -correlated trajectory predictions  $\{S_i\}_{i=1}^K$  returned by  $D_{\theta}$  to compute the  $K$ -shot vector field:

$$v_{\theta}^{(i)} = \frac{S_i - Y_i^t}{1 - t}, \quad \forall i \in [K].$$

During training, since only one future motion  $Y^1$  is observed in the dataset for a given context  $C$ , obtaining interpolated noisy data  $Y_{1:K}^t$  at arbitrary time  $t$  requires a more nuanced approach. To stabilize training, we enforce the noise to be shared among all  $K$  components. Specifically, we first draw a noise vector  $Y^0 \sim \mathcal{N}(\mathbf{0}, \mathbf{I})$  and define  $Y_i^t = (1 - t)Y^0 + tY^1, \forall i \in [K]$ , ensuring it is identical for all components. Additional analysis and ablations on MoFlow can be found in the supplementary materials. As for sampling, we initialize  $Y_i^0$  from standard normal distribution for all components to solve the ODEs.

**Time Schedule.** Similar to prior works [12, 16, 51], we find that the time schedule used during training significantly impacts model performance. The vanilla uniform distribution  $t \sim \mathcal{U}[0, 1]$  from [34, 35] performs sub-optimally on our tasks. Instead, we use a logit-normal distribution for  $t$  with  $\text{logit}(t) \sim \mathcal{N}(\mu_t, \sigma_t^2)$ ,<sup>2</sup> to better support training. In particular, the modified loss in Eq. (4.3) tends to overfit when  $t$  approaches 1, resulting in larger errors in vector field estimation at the final sample stage. Thus, we set  $\mu_t = -0.5$  and  $\sigma_t = 1.5$  to ensure that training more frequently covers the noisier regime when  $t$  is closer to 0.

<sup>2</sup>Here,  $\text{logit}(t) = \ln \frac{t}{1-t}$  is the standard logit function.

### 4.3. IMLE Distillation for MoFlow

In this section, we propose a principled distillation method for the learned MoFlow to bypass time-consuming ODE-based sampling. The approach leverages conditional implicit maximum likelihood estimation (IMLE) [31, 32] to train a student model for one-step sampling. Note that IMLE was originally proposed to train generative models that can alleviate the common mode collapse issue.

The IMLE distillation process is outlined in Algorithm 1, where we adapt this to our trajectory forecasting context. Specifically, lines 4–6 describe the standard ODE-based sampling of the teacher model, where the trained MoFlow numerically solves the ODE up to  $t = 1$ . This produces  $K$  correlated multi-modal trajectory predictions  $\hat{Y}_{1:K}^1$  conditioned on the context  $C$ . A conditional IMLE generator  $G_{\phi}$  then uses a noise vector  $Z$  and context  $C$  to stochastically generate  $K$ -component trajectories  $\Gamma \in \mathbb{R}^{K \times A \times 2T_f}$ , matching the shape of  $\hat{Y}_{1:K}^1$ .

The conditional IMLE objective generates more samples than those present in the distillation dataset for the same context  $C$ . In practice,  $m$  i.i.d. samples are generated via  $G_{\phi}$  for the same context, and the one closest to the teacher model’s prediction  $\hat{Y}_{1:K}^1$  is selected for loss computation. The objective minimizes the distance between the teacher model sample and its nearest sample from the student model using the distance metric  $\mathcal{L}_{\text{IMLE}}$ , ensuring that the teacher model data mode is closely approximated by at least one sample from the student model. To preserve trajectory prediction multi-modality, we employ the Chamfer distance [33] as the loss function  $\mathcal{L}_{\text{IMLE}}$ , which measures the similarity between two sets of trajectories across all agents:

$$\mathcal{L}_{\text{IMLE}}(\hat{Y}_{1:K}^1, \Gamma) = \frac{1}{K} \left( \sum_{i=1}^K \min_j \|\hat{Y}_i^1 - \Gamma^{(j)}\| + \sum_{j=1}^K \min_i \|\hat{Y}_i^1 - \Gamma^{(j)}\| \right),$$

where  $\Gamma^{(i)} \in \mathbb{R}^{A \times 2T_f}$  is the  $i$ -th component of the IMLE-generated correlated trajectory.

**Efficient and Flexible Distillation.** The IMLE framework provides an efficient and flexible solution for flow model distillation. Its backbone, denoted by  $G_{\phi}$ , is architecturally unrestricted and can share the same architecture as the teacher model (except for eliminating time step embeddings), as both teacher and student models aim to learn spatio-temporal dependencies. Moreover, IMLE is inherently stable compared to adversarial models like GANs, avoiding mode collapse and vanishing gradients [31, 32]. Compared to existing deterministic methods [45], IMLE employs a principled probabilistic approach [31, 32], enhancing robustness and flexibility.

Table 1. Comparison with baseline models on **NBA** dataset.  $\min_{20}\text{ADE}/\min_{20}\text{FDE}$  (meters) are reported. Bold/underlined fonts represent the best/second-best result. For LED, we denote its stage-one DDPM model as LED<sup>†</sup> and the results from the LED initializer as LED\*.

Time	MemoNet [74]	NPSN [4]	GroupNet [73]	MID [18]	LED <sup>†</sup> [45]	LED* [45]	MoFlow	IMLE
1.0s	0.38/0.56	0.35/0.58	0.26/0.34	0.28/0.37	<u>0.21/0.28</u>	<b>0.18/0.27</b>	<b>0.18/0.25</b>	<b>0.18/0.25</b>
2.0s	0.71/1.14	0.68/1.23	0.49/0.70	0.51/0.72	<u>0.44/0.64</u>	<u>0.37/0.56</u>	<b>0.34/0.47</b>	<b>0.34/0.47</b>
3.0s	1.00/1.57	1.01/1.76	0.73/1.02	0.71/0.98	0.69/0.95	<u>0.58/0.84</u>	<b>0.52/0.67</b>	<b>0.52/0.67</b>
Total (4.0s)	1.25/1.47	1.31/1.79	0.96/1.30	0.96/1.27	0.94/1.21	<u>0.81/1.16</u>	<b>0.71/0.87</b>	<b>0.71/0.86</b>

Table 2. Comparison with baseline distillation models on **ETH-UCY** dataset.  $\min_{20}\text{ADE}/\min_{20}\text{FDE}$  (meters) are reported. Bold/underlined fonts represent the best/second-best result. LED\* represents the results from student model LED initializer.

Subsets	MID [18]	GroupNet [73]	TUTR [56]	EqMotion [75]	EigenTraj [5]	LED* [45]	SingularTraj [6]	MoFlow	IMLE
ETH	0.39/0.66	0.46/0.73	0.40/0.61	0.40/0.61	<u>0.36/0.53</u>	0.39/0.58	<b>0.35/0.42</b>	0.40/0.57	0.40/0.58
HOTEL	0.13/0.22	0.15/0.25	<b>0.11/0.18</b>	<u>0.12/0.18</u>	<u>0.12/0.19</u>	<b>0.11/0.17</b>	0.13/0.19	<b>0.11/0.17</b>	0.12/0.18
UNIV	<b>0.22/0.45</b>	0.26/0.49	<u>0.23/0.42</u>	<u>0.23/0.43</u>	0.24/0.34	0.26/0.44	0.25/0.44	<u>0.23/0.39</u>	<u>0.23/0.39</u>
ZARA1	0.17/0.30	0.21/0.39	0.18/0.34	0.18/ <u>0.32</u>	0.19/0.33	0.18/ <b>0.26</b>	0.19/0.32	<b>0.15/0.26</b>	<u>0.16/0.26</u>
ZARA2	<u>0.13/0.27</u>	0.17/0.33	<u>0.13/0.25</u>	<u>0.13/0.23</u>	0.14/0.24	<u>0.13/0.22</u>	0.15/0.25	<b>0.12/0.22</b>	<u>0.13/0.22</u>
AVG	<u>0.21/0.38</u>	0.25/0.44	<u>0.21/0.36</u>	<u>0.21/0.35</u>	<u>0.21/0.34</u>	<u>0.21/0.33</u>	<u>0.21/0.32</u>	<b>0.20/0.32</b>	<u>0.21/0.33</u>

## 5. Experiments

### 5.1. Datasets and Metrics

We evaluate our method on three human motion prediction datasets, including one sports dataset (NBA) and two pedestrian datasets (ETH-UCY and Stanford Drone Dataset).

**NBA Dataset.** The NBA SportVU dataset tracks the trajectories of 10 players and the ball during NBA basketball games. Each game segment has a fixed number of agents. In this task, we predict 20 future frames (4.0s) using 10 past frames (2.0s) as input.

**ETH-UCY Datasets.** The ETH-UCY datasets include 1,536 pedestrians across five distinct scenes: ETH, Hotel, Univ, Zara1, and Zara2. These trajectories, recorded from surveillance viewpoints, are labeled in world coordinates, encompassing a range of motion patterns. We use an 8-second segment length to align with the previous works [18, 45], where 8 frames (3.2s) of past trajectories are used to forecast future 12 frames (4.8s). For evaluation, we adopt a leave-one-out approach, training on four scenes and using the remaining scene for testing.

**SDD dataset.** The Stanford Drone Dataset (SDD) is a massive pedestrian dataset captured from a bird’s-eye view on a university campus. Following prior studies [18, 45, 56], we use the standard train-test split, utilizing 8 frames (3.2s) of past observations to predict the subsequent 12 frames (4.8s).

**Evaluation Metrics.** 1) Minimum Average Displacement Error ( $\min_K\text{ADE}$ ) computes the minimum Euclidean average distance overall estimated positions in the  $K$  predicted

trajectories and the ground-truth. 2) Minimum Final Displacement Error ( $\min_K\text{FDE}$ ) delineates the minimum Euclidean distance between the ground-truth final destination and the final destination of  $K$  predicted trajectories.

### 5.2. Implementation Details

In our approach, trajectories are preprocessed using min-max normalization to scale future relative motions to the range  $[-1, 1]$  to stabilize training dynamics. The backbone of our method is a standard transformer architecture [64], which is augmented with sinusoidal positional encodings to capture inter-agent spatial relationships. These encodings are applied at both the agent and prediction levels, with self-attention alternately operating across these levels to reinforce agent interactions and enhance scene coherence. The teacher model generates samples through a 100-step denoising ODE process, and these precomputed samples are subsequently used to evaluate performance and to train the student model via the IMLE objective. The student model retains the same architectural structure as the teacher, except that it omits the flow time positional encoding layers. Further details are provided in Appendix A.5.

### 5.3. Baselines

We compare our MoFlow model and IMLE distillation method with state-of-the-art approaches, including MemoNet [74], NPSN [4], GroupNet [73], MID [18], LED [45], TUTR [56], EqMotion [75], EigenTraj [5], SingularTraj [6], Evo-Graph [30], Y-net [44], CAGN [11], and SocialVAE [77], on datasets where comparable results are readily

Table 3. Comparison with state-of-the-art methods on the SDD dataset in  $\min_{20}\text{ADE}/\min_{20}\text{FDE}$  (pixels).

Method	Venue	ADE/FDE
Evo-Graph [30]	NIPS’20	13.90/22.90
Y-net [44]	ICCV’21	11.49/20.23
GroupNet [73]	CVPR’22	9.31/16.11
CAGN [11]	AAAI’22	9.42/15.93
NPSN [4]	CVPR’22	8.56/11.85
MemoNet [74]	CVPR’22	9.50/14.78
SocialVAE [77]	ECCV’22	8.88/14.81
MID [18]	CVPR’22	9.73/15.32
TUTR [56]	ICCV’23	7.76/12.69
EigenTraj [5]	ICCV’23	8.05/13.25
LED [45]	CVPR’23	8.48/11.66
ET+HighGraph [26]	CVPR’24	7.81/11.09
<b>MoFlow</b>	-	<b>7.50/11.96</b>
<b>IMLE</b>	-	<b>7.85/12.86</b>

available. In terms of LED [45], we reproduce the results using its codebase, while the outcomes for the remaining models are directly extracted from their respective papers.

## 5.4. Quantitative Results

We present our model’s state-of-the-art quantitative results in Tab. 1, Tab. 2, and Tab. 3 across three datasets. As shown in Tab. 1, both our teacher and student methods significantly outperform other baseline models on the NBA dataset, achieving 0.71 minADE and 0.87 minFDE—improvements of over 12% and 25%, respectively, compared to the previous state-of-the-art method. On the ETH-UCY datasets, our methods deliver performance comparable to the best existing models. It is worth noting that the performance on the ETH-UCY datasets has plateaued in recent years due to the datasets’ size and the rapid advancement of expressive models. Nonetheless, our models successfully match the performance of the best available methods. On the SDD dataset in Tab. 3, our models achieve state-of-the-art performance on the minADE metric and competitive results on the minFDE metric, coming within 0.5 of the best model.

Notably, with our IMLE distillation, the final performance remains largely unchanged among all three datasets. This is particularly significant, as one-step generation eliminates the need for the time-consuming denoising ODE solving process, which is 100 times faster in our current setup. The retained performance indicates that iterative denoising steps can be effectively removed, enabling faster sampling during deployment. More results about inference time and performance are included in Tab. 9 of the supplement.

Table 4. Comparison with different distillation methods on NBA dataset.  $\min_{20}\text{ADE}/\min_{20}\text{FDE}$  are reported. All the models learn to generate samples conforming to the marginal distribution from teacher model samples at time step  $t = 1$ .

Time	MoFlow-IMLE	WGAN [3]	DCGAN [53]
1.0s	0.18/0.25	0.35/0.58	0.33/0.60
2.0s	0.35/0.47	0.74/1.56	0.72/1.64
3.0s	0.52/0.67	1.30/2.30	1.22/2.31
Total (4.0s)	0.71/0.87	1.78/2.90	1.71/2.98

## 5.5. Qualitative Results

We illustrate our model’s performance by visualizing the predicted trajectories on the NBA sports dataset and ETH-UCY pedestrian dataset. Consider Sec. 5.3, our MoFlow IMLE predicts more accurate results than the LED model, which aligns to the results in Tab. 1. In Sec. 5.3, the diverse predicted trajectories of professional basketball player and basketball are showcased. Likewise, as demonstrated in the scenarios from the ETH-UCY dataset in Fig. 4, our predictions frequently align with the ground-truth pedestrian trajectories. Note that we employ two versions of the ETH-UCY dataset. The results reported in Tab. 2 are based on the dataset versions utilized in MID [18] and LED [45]. In contrast, we present the qualitative result Fig. 4 using the ETH-UCY test set from SocialGAN[19], following the same data split. Moreover, the quantitative results for this version are provided in Tab. 8 of the Supplementary Material.

## 5.6. Ablation Studies

Regarding the IMLE objective, we conduct a comparative analysis using DCGAN [53] and WGAN [3] as baseline implicit models in Tab. 4. GAN-based distillation methods fail to deliver satisfactory performance due to their inherent training instability. In contrast, the IMLE training objective is both fast and stable, achieving state-of-the-art performance compared to existing baselines, as shown in Tab. 1.

## 6. Conclusion

This paper presents a novel MoFlow model for trajectory prediction tasks. Our new flow matching loss effectively learns a diverse set of future trajectories, addressing the inherent multi-modality of human motion. Additionally, we propose the first one-step IMLE distillation model, which involves a process to strategically match the multi-modal future trajectories through a latent variable. This distillation method ameliorates the trilemma [71] in generative learning, enabling the fast generation of accurate and diverse future trajectories. Our approach demonstrates strong performance, delivering results that are competitive with, and in some aspects surpass, those of current state-of-the-art models, as evidenced by our evaluations on the NBA SportVU,

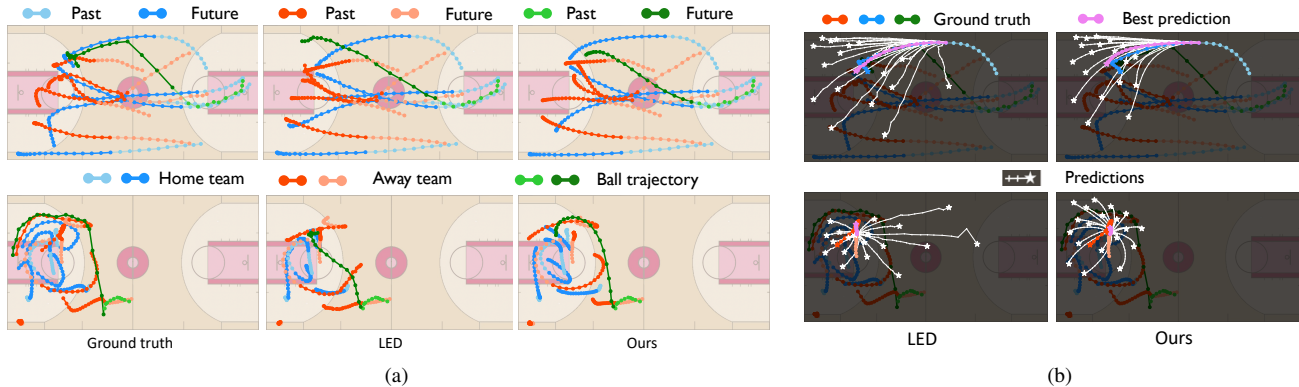


Figure 3. Qualitative results on the NBA dataset. (a) We compare between the best-of-20 predictions from our MoFlow IMLE distillation method, the best-of-20 predictions the LED method, and the ground truth future trajectories. The visualization demonstrates that our approach produces predictions that more closely align with the ground truth trajectories compared to the LED model. (b) We are using two same scenes as (a). This figure delineates the diversity of samples from our IMLE generator. Our method generates a prediction that conforms to the GT trajectory. (Pink: the sample closest to the ground truth in  $L_2$  sense among  $K = 20$  predictions.)

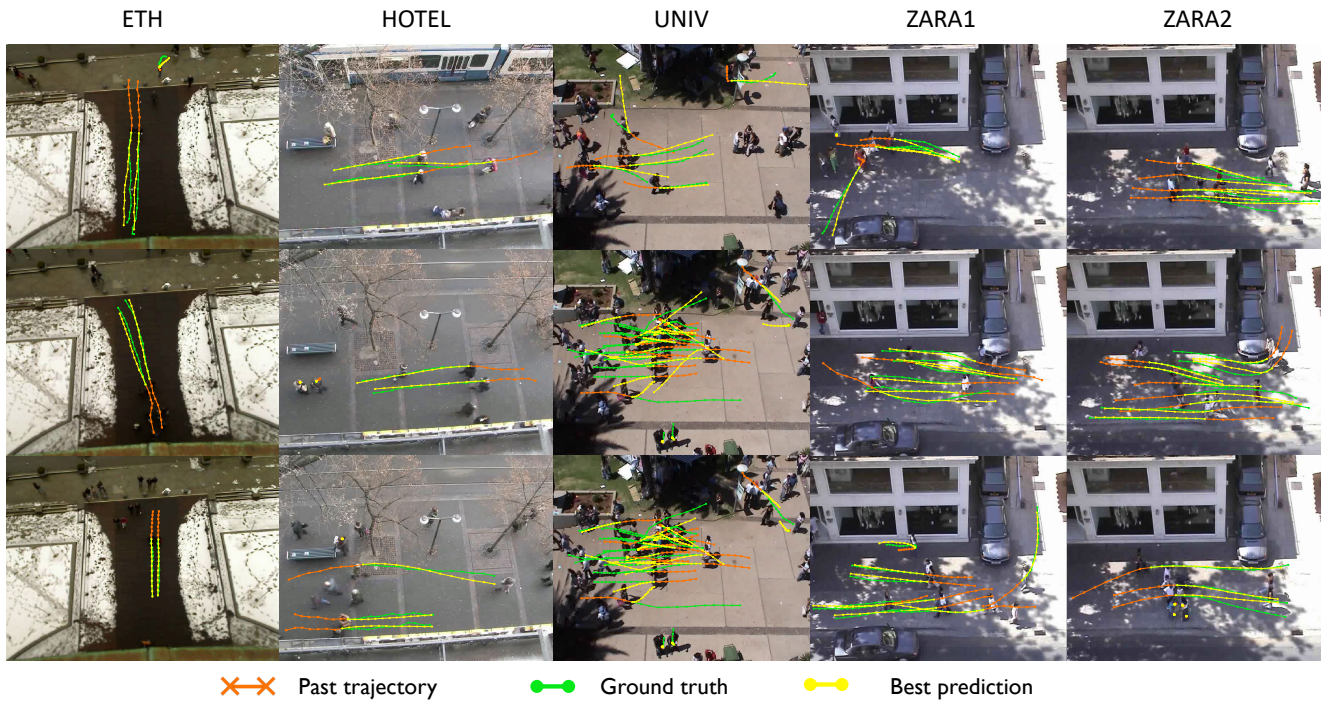


Figure 4. The qualitative results on the ETH-UCY dataset show that our MoFlow IMLE distillation model’s best-of-20 predictions (selected via the lowest FDE) closely match the ground truth future trajectories, capturing important motion nuances.

ETH-UCY and SDD datasets. Our distilled student model achieves a 100-fold increase in sampling speed due to its one-step prediction mechanism. This underscores the potential of the IMLE distillation model as a step forward in the field of stochastic trajectory forecasting, providing both efficiency and effectiveness in generative learning tasks.

**Future work.** One possible direction is to leverage semantic maps and scene graphs to encode environmental features

such as lanes, sidewalks, and obstacles directly into the model. These structured representations enrich contextual understanding, improving the model’s capability to generate trajectories that are both context-aware and constraint-compliant. Furthermore, this approach can be extended to large-scale autonomous driving datasets, broadening its applicability and robustness.



## Acknowledgment

This work was funded, in part, by the NSERC Discovery Grants (No. RGPIN-2022-04636, RGPIN-2019-05448, and RGPIN-2021-04012), the Vector Institute for AI, and Canada CIFAR AI Chair. Resources used in preparing this research were provided, in part, by the Province of Ontario, the Government of Canada through the Digital Research Alliance of Canada [alliance.ca](http://alliance.ca), and companies sponsoring the Vector Institute [www.vectorinstitute.ai/#partners](http://www.vectorinstitute.ai/#partners), and Advanced Research Computing at University of British Columbia. Additional hardware support was provided by John R. Evans Leaders Fund CFI grant.

## References

- [1] Josh Abramson, Jonas Adler, Jack Dunger, Richard Evans, Tim Green, Alexander Pritzel, Olaf Ronneberger, Lindsay Willmore, Andrew J Ballard, Joshua Babrick, et al. Accurate structure prediction of biomolecular interactions with alphafold 3. *Nature*, pages 1–3, 2024. 2
- [2] Michael S Albergo, Nicholas M Boffi, and Eric Vanden-Eijnden. Stochastic interpolants: A unifying framework for flows and diffusions. *arXiv preprint arXiv:2303.08797*, 2023. 1, 2, 3
- [3] Martin Arjovsky, Soumith Chintala, and Léon Bottou. Wasserstein generative adversarial networks. In *International conference on machine learning*, pages 214–223. PMLR, 2017. 7
- [4] Inhwan Bae, Jin-Hwi Park, and Hae-Gon Jeon. Non-probability sampling network for stochastic human trajectory prediction. In *Proceedings of the IEEE/CVF Conference on Computer Vision and Pattern Recognition (CVPR)*, pages 6477–6487, 2022. 6, 7
- [5] Inhwan Bae, Jean Oh, and Hae-Gon Jeon. Eigentrajectory: Low-rank descriptors for multi-modal trajectory forecasting. In *Proceedings of the IEEE/CVF International Conference on Computer Vision*, 2023. 6, 7, 18
- [6] Inhwan Bae, Young-Jae Park, and Hae-Gon Jeon. Singulartrajectory: Universal trajectory predictor using diffusion model. In *Proceedings of the IEEE/CVF Conference on Computer Vision and Pattern Recognition*, 2024. 1, 6, 18
- [7] Omer Bar-Tal, Hila Chefer, Omer Tov, Charles Herrmann, Roni Paiss, Shiran Zada, Ariel Ephrat, Junhwa Hur, Guanghui Liu, Amit Raj, et al. Lumiere: A space-time diffusion model for video generation. In *SIGGRAPH Asia 2024 Conference Papers*, pages 1–11, 2024. 2
- [8] David Berthelot, Arnaud Autef, Jierui Lin, Dian Ang Yap, Shuangfei Zhai, Siyuan Hu, Daniel Zheng, Walter Talbott, and Eric Gu. Tract: Denoising diffusion models with transitive closure time-distillation. *arXiv preprint arXiv:2303.04248*, 2023. 2
- [9] Apratim Bhattacharyya, Michael Hanselmann, Mario Fritz, Bernt Schiele, and Christoph-Nikolas Straehle. Conditional flow variational autoencoders for structured sequence prediction. *arXiv preprint arXiv:1908.09008*, *Bayesian Deep Learning and Machine Learning for Autonomous Driving NeurIPS*, 2019. 2
- [10] Patrick Dendorfer, Sven Elflein, and Laura Leal-Taixé. Mg-gan: A multi-generator model preventing out-of-distribution samples in pedestrian trajectory prediction. In *Proceedings of the IEEE/CVF International Conference on Computer Vision*, pages 13158–13167, 2021. 1, 2
- [11] Jinghai Duan, Le Wang, Chengjiang Long, Sanping Zhou, Fang Zheng, Liushuai Shi, and Gang Hua. Complementary attention gated network for pedestrian trajectory prediction. *Proceedings of the AAAI Conference on Artificial Intelligence*, 36(1):542–550, 2022. 6, 7
- [12] Patrick Esser, Sumith Kulal, Andreas Blattmann, Rahim Entezari, Jonas Müller, Harry Saini, Yam Levi, Dominik Lorenz, Axel Sauer, Frederic Boesel, et al. Scaling rectified flow transformers for high-resolution image synthesis. In *Forty-first International Conference on Machine Learning*, 2024. 5, 15
- [13] Scott Ettinger, Shuyang Cheng, Benjamin Caine, Chenxi Liu, Hang Zhao, Sabeek Pradhan, Yuning Chai, Ben Sapp, Charles R Qi, Yin Zhou, et al. Large scale interactive motion forecasting for autonomous driving: The waymo open motion dataset. In *Proceedings of the IEEE/CVF International Conference on Computer Vision*, pages 9710–9719, 2021. 1
- [14] Dario Floreano and Robert J Wood. Science, technology and the future of small autonomous drones. *nature*, 521(7553):460–466, 2015. 1
- [15] Kevin Frans, Danijar Hafner, Sergey Levine, and Pieter Abbeel. One step diffusion via shortcut models. In *The Thirteenth International Conference on Learning Representations*, 2025. 2
- [16] Itai Gat, Tal Remez, Neta Shaul, Felix Kreuk, Ricky TQ Chen, Gabriel Synnaeve, Yossi Adi, and Yaron Lipman. Discrete flow matching. *Advances in Neural Information Processing Systems*, 37:133345–133385, 2025. 2, 5
- [17] Jiatao Gu, Shuangfei Zhai, Yizhe Zhang, Lingjie Liu, and Joshua M Susskind. Boot: Data-free distillation of denoising diffusion models with bootstrapping. In *ICML 2023 Workshop on Structured Probabilistic Inference and Generative Modeling*, 2023. 2

- [18] Tianpei Gu, Guangyi Chen, Junlong Li, Chunze Lin, Yongming Rao, Jie Zhou, and Jiwen Lu. Stochastic trajectory prediction via motion indeterminacy diffusion. In *Proceedings of the IEEE/CVF Conference on Computer Vision and Pattern Recognition (CVPR)*, pages 17113–17122, 2022. 1, 2, 4, 6, 7, 16, 18
- [19] Agrim Gupta, Justin Johnson, Li Fei-Fei, Silvio Savarese, and Alexandre Alahi. Social gan: Socially acceptable trajectories with generative adversarial networks. In *Proceedings of the IEEE conference on computer vision and pattern recognition*, pages 2255–2264, 2018. 2, 7, 18
- [20] Geoffrey Hinton, Oriol Vinyals, and Jeff Dean. Distilling the knowledge in a neural network. *arXiv preprint arXiv:1503.02531*, 2015. 2
- [21] Jonathan Ho, Ajay Jain, and Pieter Abbeel. Denoising diffusion probabilistic models. *Advances in neural information processing systems*, 33:6840–6851, 2020. 2, 3
- [22] Jonathan Ho, Tim Salimans, Alexey Gritsenko, William Chan, Mohammad Norouzi, and David J Fleet. Video diffusion models. *Advances in Neural Information Processing Systems*, 35:8633–8646, 2022. 2
- [23] Ajay Jain, Sergio Casas, Renjie Liao, Yuwen Xiong, Song Feng, Sean Segal, and Raquel Urtasun. Discrete residual flow for probabilistic pedestrian behavior prediction. In *Conference on Robot Learning*, pages 407–419. PMLR, 2020. 1
- [24] Chiyu Jiang, Andre Cornman, Cheolho Park, Benjamin Sapp, Yin Zhou, Dragomir Anguelov, et al. Motiondiffuser: Controllable multi-agent motion prediction using diffusion. In *Proceedings of the IEEE/CVF Conference on Computer Vision and Pattern Recognition*, pages 9644–9653, 2023. 4
- [25] Beomsu Kim, Yu-Guan Hsieh, Michal Klein, marco cuturi, Jong Chul Ye, Bahjat Kawar, and James Thornton. Simple reflow: Improved techniques for fast flow models. In *The Thirteenth International Conference on Learning Representations*, 2025. 2
- [26] Sungjune Kim, Hyung-gun Chi, Hyerin Lim, Karthik Ramani, Jinkyu Kim, and Sangpil Kim. Higher-order relational reasoning for pedestrian trajectory prediction. In *Proceedings of the IEEE/CVF Conference on Computer Vision and Pattern Recognition (CVPR)*, pages 15251–15260, 2024. 7
- [27] Durk P Kingma and Prafulla Dhariwal. Glow: Generative flow with invertible 1x1 convolutions. *Advances in neural information processing systems*, 31, 2018. 1
- [28] Marcel Kollovich, Abdul Fatir Ansari, Michael Bohlke-Schneider, Jasper Zschiegner, Hao Wang, and Bernie Wang. Predict, refine, synthesize: Self-guiding diffusion models for probabilistic time series forecasting. In *Thirty-seventh Conference on Neural Information Processing Systems*, 2023. 1
- [29] Mihee Lee, Samuel S. Sohn, Seonghyeon Moon, Sejong Yoon, Mubbasir Kapadia, and Vladimir Pavlovic. Muse-vae: Multi-scale vae for environment-aware long term trajectory prediction. In *Proceedings of the IEEE/CVF Conference on Computer Vision and Pattern Recognition (CVPR)*, pages 2221–2230, 2022. 1, 2
- [30] Jiachen Li, Fan Yang, Masayoshi Tomizuka, and Chiho Choi. Evolvegraph: Multi-agent trajectory prediction with dynamic relational reasoning. In *Proceedings of the Neural Information Processing Systems (NeurIPS)*, 2020. 6, 7
- [31] Ke Li and Jitendra Malik. Implicit maximum likelihood estimation. *arXiv preprint arXiv:1809.09087*, 2018. 2, 5
- [32] Ke Li, Tianhao Zhang, and Jitendra Malik. Diverse image synthesis from semantic layouts via conditional imle. In *Proceedings of the IEEE international conference on computer vision*, 2019. 5
- [33] Fangzhou Lin, Yun Yue, Ziming Zhang, Songlin Hou, Kazunori Yamada, Vijaya Kolachalama, and Venkatesh Saligrama. Infocd: A contrastive chamfer distance loss for point cloud completion. In *Advances in Neural Information Processing Systems*, pages 76960–76973. Curran Associates, Inc., 2023. 5
- [34] Yaron Lipman, Ricky TQ Chen, Heli Ben-Hamu, Maximilian Nickel, and Matt Le. Flow matching for generative modeling. *arXiv preprint arXiv:2210.02747*, 2022. 1, 2, 3, 4, 5
- [35] Xingchao Liu, Chengyue Gong, and Qiang Liu. Flow straight and fast: Learning to generate and transfer data with rectified flow. *arXiv preprint arXiv:2209.03003*, 2022. 1, 2, 3, 5
- [36] Xingchao Liu, Xiwen Zhang, Jianzhu Ma, Jian Peng, and Qiang Liu. InstafLOW: One step is enough for high-quality diffusion-based text-to-image generation. In *International Conference on Learning Representations*, 2024. 2
- [37] Yuejiang Liu, Qi Yan, and Alexandre Alahi. Social nce: Contrastive learning of socially-aware motion representations. In *Proceedings of the IEEE/CVF International Conference on Computer Vision*, pages 15118–15129, 2021. 1
- [38] Ilya Loshchilov and Frank Hutter. Decoupled weight decay regularization. In *International Conference on Learning Representations*, 2019. 16
- [39] Cheng Lu, Yuhao Zhou, Fan Bao, Jianfei Chen, Chongxuan Li, and Jun Zhu. Dpm-solver++: Fast solver for guided sampling of diffusion probabilistic models, 2023. 2

- [40] Eric Luhman and Troy Luhman. Knowledge distillation in iterative generative models for improved sampling speed. *arXiv preprint arXiv:2101.02388*, 2021. [2](#)
- [41] Katie Luo, Sergio Casas, Renjie Liao, Xinchun Yan, Yuwen Xiong, Wenyuan Zeng, and Raquel Urtasun. Safety-oriented pedestrian occupancy forecasting. In *2021 IEEE/RSJ International Conference on Intelligent Robots and Systems (IROS)*, pages 1015–1022. IEEE, 2021. [1](#)
- [42] Weijian Luo. A comprehensive survey on knowledge distillation of diffusion models. *arXiv preprint arXiv:2304.04262*, 2023. [2](#)
- [43] Weijian Luo, Tianyang Hu, Shifeng Zhang, Jiacheng Sun, Zhenguo Li, and Zhihua Zhang. Diff-instruct: A universal approach for transferring knowledge from pre-trained diffusion models. *Advances in Neural Information Processing Systems*, 36:76525–76546, 2023. [3](#)
- [44] Karttikeya Mangalam, Yang An, Harshayu Girase, and Jitendra Malik. From goals, waypoints & paths to long term human trajectory forecasting. In *Proc. International Conference on Computer Vision (ICCV)*, 2021. [6, 7](#)
- [45] Weibo Mao, Chenxin Xu, Qi Zhu, Siheng Chen, and Yanfeng Wang. Leapfrog diffusion model for stochastic trajectory prediction. In *Proceedings of the IEEE/CVF Conference on Computer Vision and Pattern Recognition (CVPR)*, pages 5517–5526, 2023. [1, 2, 3, 4, 5, 6, 7, 16, 17, 18](#)
- [46] Andrew Melnik, Michal Ljubicjanac, Cong Lu, Qi Yan, Weiming Ren, and Helge Ritter. Video diffusion models: A survey. *arXiv preprint arXiv:2405.03150*, 2024. [2](#)
- [47] Chenlin Meng, Robin Rombach, Ruiqi Gao, Diederik Kingma, Stefano Ermon, Jonathan Ho, and Tim Salimans. On distillation of guided diffusion models. In *Proceedings of the IEEE/CVF Conference on Computer Vision and Pattern Recognition (CVPR)*, pages 14297–14306, 2023. [2](#)
- [48] Nigamaa Nayakanti, Rami Al-Rfou, Aurick Zhou, Kratharth Goel, Khaled S Refaat, and Benjamin Sapp. Wayformer: Motion forecasting via simple & efficient attention networks. In *2023 IEEE International Conference on Robotics and Automation (ICRA)*, pages 2980–2987. IEEE, 2023. [1](#)
- [49] Jiquan Ngiam, Vijay Vasudevan, Benjamin Caine, Zhengdong Zhang, Hao-Tien Lewis Chiang, Jeffrey Ling, Rebecca Roelofs, Alex Bewley, Chenxi Liu, Ashish Venugopal, et al. Scene transformer: A unified architecture for predicting future trajectories of multiple agents. In *International Conference on Learning Representations*, 2021. [16](#)
- [50] Adam Paszke, Sam Gross, Francisco Massa, Adam Lerer, James Bradbury, Gregory Chanan, Trevor Killeen, Zeming Lin, Natalia Gimelshein, Luca Antiga, et al. Pytorch: An imperative style, high-performance deep learning library. *Advances in neural information processing systems*, 32, 2019. [16](#)
- [51] Adam Polyak, Amit Zohar, Andrew Brown, Andros Tjandra, Animesh Sinha, Ann Lee, Apoorv Vyas, Bowen Shi, Chih-Yao Ma, Ching-Yao Chuang, et al. Movie gen: A cast of media foundation models. *arXiv preprint arXiv:2410.13720*, 2024. [2, 5, 15](#)
- [52] Charles R Qi, Hao Su, Kaichun Mo, and Leonidas J Guibas. Pointnet: Deep learning on point sets for 3d classification and segmentation. In *Proceedings of the IEEE conference on computer vision and pattern recognition*, pages 652–660, 2017. [16](#)
- [53] Alec Radford, Luke Metz, and Soumith Chintala. Unsupervised representation learning with deep convolutional generative adversarial networks. *arXiv preprint arXiv:1511.06434*, 2016. [7](#)
- [54] Amir Sadeghian, Vineet Kosaraju, Ali Sadeghian, Noriaki Hirose, Hamid Rezaatofghi, and Silvio Savarese. Sophie: An attentive gan for predicting paths compliant to social and physical constraints. In *Proceedings of the IEEE/CVF conference on computer vision and pattern recognition*, pages 1349–1358, 2019. [2](#)
- [55] Axel Sauer, Dominik Lorenz, Andreas Blattmann, and Robin Rombach. Adversarial diffusion distillation. In *European Conference on Computer Vision*, pages 87–103. Springer, 2024. [3](#)
- [56] Liushuai Shi, Le Wang, Sanping Zhou, and Gang Hua. Trajectory unified transformer for pedestrian trajectory prediction. In *Proceedings of the IEEE/CVF International Conference on Computer Vision (ICCV)*, pages 9675–9684, 2023. [6, 7, 18](#)
- [57] Jascha Sohl-Dickstein, Eric Weiss, Niru Maheswaranathan, and Surya Ganguli. Deep unsupervised learning using nonequilibrium thermodynamics. In *Proceedings of the 32nd International Conference on Machine Learning*, pages 2256–2265, Lille, France, 2015. [2, 3](#)
- [58] Jiaming Song, Chenlin Meng, and Stefano Ermon. Denoising diffusion implicit models. *arXiv preprint arXiv:2010.02502*, 2020. [2, 3](#)
- [59] Yang Song and Stefano Ermon. Generative modeling by estimating gradients of the data distribution. In *Advances in Neural Information Processing Systems*. Curran Associates, Inc., 2019. [2](#)
- [60] Yang Song, Jascha Sohl-Dickstein, Diederik P Kingma, Abhishek Kumar, Stefano Ermon, and Ben Poole. Score-based generative modeling through stochastic differential equations. In *International Conference on Learning Representations*, 2021. [2, 3](#)

- [61] Yang Song, Prafulla Dhariwal, Mark Chen, and Ilya Sutskever. Consistency models. *arXiv preprint arXiv:2303.01469*, 2023. 2
- [62] Simon Suo, Sebastian Regalado, Sergio Casas, and Raquel Urtasun. Trafficsim: Learning to simulate realistic multi-agent behaviors. In *Proceedings of the IEEE/CVF Conference on Computer Vision and Pattern Recognition*, pages 10400–10409, 2021. 17
- [63] Jonathan Ho Tim Salimans. Progressive distillation for fast sampling of diffusion models. In *International Conference on Learning Representations*, 2021. 2
- [64] Ashish Vaswani, Noam Shazeer, Niki Parmar, Jakob Uszkoreit, Llion Jones, Aidan N Gomez, Łukasz Kaiser, and Illia Polosukhin. Attention is all you need. *Advances in neural information processing systems*, 30, 2017. 4, 6
- [65] Zhengyi Wang, Cheng Lu, Yikai Wang, Fan Bao, Chongxuan Li, Hang Su, and Jun Zhu. Prolificdreamer: High-fidelity and diverse text-to-3d generation with variational score distillation. *Advances in Neural Information Processing Systems*, 36:8406–8441, 2023. 3
- [66] Erica Weng, Hana Hoshino, Deva Ramanan, and Kris Kitani. Joint metrics matter: A better standard for trajectory forecasting. In *Proceedings of the IEEE/CVF International Conference on Computer Vision*, pages 20315–20326, 2023. 17, 19
- [67] Conghao Wong, Beihao Xia, Ziqian Zou, Yulong Wang, and Xinge You. Socialcircle: Learning the angle-based social interaction representation for pedestrian trajectory prediction. In *Proceedings of the IEEE/CVF Conference on Computer Vision and Pattern Recognition*, pages 19005–19015, 2024. 2
- [68] Lemeng Wu, Dilin Wang, Chengyue Gong, Xingchao Liu, Yunyang Xiong, Rakesh Ranjan, Raghuraman Krishnamoorthi, Vikas Chandra, and Qiang Liu. Fast point cloud generation with straight flows. In *Proceedings of the IEEE/CVF Conference on Computer Vision and Pattern Recognition (CVPR)*, pages 9445–9454, 2023. 2
- [69] Zike Wu, Pan Zhou, Kenji Kawaguchi, and Hanwang Zhang. Fast diffusion model. *arXiv preprint arXiv:2306.06991*, 2023. 2
- [70] Zike Wu, Pan Zhou, Xuanyu Yi, Xiaoding Yuan, and Hanwang Zhang. Consistent3d: Towards consistent high-fidelity text-to-3d generation with deterministic sampling prior, 2024. 2
- [71] Zhisheng Xiao, Karsten Kreis, and Arash Vahdat. Tackling the generative learning trilemma with denoising diffusion GANs. In *International Conference on Learning Representations (ICLR)*, 2022. 3, 7
- [72] Sirui Xie, Zhisheng Xiao, Diederik P. Kingma, Tingbo Hou, Ying Nian Wu, Kevin Patrick Murphy, Tim Salimans, Ben Poole, and Ruiqi Gao. Em distillation for one-step diffusion models. *ArXiv*, abs/2405.16852, 2024. 3
- [73] Chenxin Xu, Maosen Li, Zhenyang Ni, Ya Zhang, and Siheng Chen. Groupnet: Multiscale hypergraph neural networks for trajectory prediction with relational reasoning. In *Proceedings of the IEEE/CVF Conference on Computer Vision and Pattern Recognition (CVPR)*, pages 6498–6507, 2022. 1, 2, 6, 7, 18
- [74] Chenxin Xu, Weibo Mao, Wenjun Zhang, and Siheng Chen. Remember intentions: Retrospective-memory-based trajectory prediction. In *Proceedings of the IEEE/CVF Conference on Computer Vision and Pattern Recognition (CVPR)*, pages 6488–6497, 2022. 6, 7
- [75] Chenxin Xu, Robby T Tan, Yuhong Tan, Siheng Chen, Yu Guang Wang, Xinchao Wang, and Yanfeng Wang. Eqmotion: Equivariant multi-agent motion prediction with invariant interaction reasoning. In *Proceedings of the IEEE/CVF Conference on Computer Vision and Pattern Recognition*, pages 1410–1420, 2023. 6, 18
- [76] Chenxin Xu, Yuxi Wei, Bohan Tang, Sheng Yin, Ya Zhang, Siheng Chen, and Yanfeng Wang. Dynamic-group-aware networks for multi-agent trajectory prediction with relational reasoning. *Neural Networks*, 170:564–577, 2024. 1, 2
- [77] Pei Xu, Jean-Bernard Hayet, and Ioannis Karamouzas. Socialvae: Human trajectory prediction using time-wise latents. In *European Conference on Computer Vision*, pages 511–528. Springer, 2022. 6, 7
- [78] Qi Yan, Zhengyang Liang, Yang Song, Renjie Liao, and Lele Wang. Swingnn: Rethinking permutation invariance in diffusion models for graph generation. *arXiv preprint arXiv:2307.01646*, 2023. 2
- [79] Tianwei Yin, Michaël Gharbi, Richard Zhang, Eli Shechtman, Fredo Durand, William T Freeman, and Taesung Park. One-step diffusion with distribution matching distillation. In *Proceedings of the IEEE/CVF Conference on Computer Vision and Pattern Recognition*, pages 6613–6623, 2024. 3
- [80] Tianwei Yin, Michaël Gharbi, Taesung Park, Richard Zhang, Eli Shechtman, Fredo Durand, and Bill Freeman. Improved distribution matching distillation for fast image synthesis. *Advances in Neural Information Processing Systems*, 37:47455–47487, 2025. 3
- [81] Ye Yuan and Kris M. Kitani. Diverse trajectory forecasting with determinantal point processes. In *International Conference on Learning Representations*, 2020. 17
- [82] Ye Yuan, Xinshuo Weng, Yanglan Ou, and Kris Kitani. Agentformer: Agent-aware transformers for socio-temporal multi-agent forecasting. In *Proceed-*

- ings of the IEEE/CVF International Conference on Computer Vision (ICCV)*, 2021. 16
- [83] Xiaohui Zeng, Arash Vahdat, Francis Williams, Zan Gojcic, Or Litany, Sanja Fidler, and Karsten Kreis. Lion: Latent point diffusion models for 3d shape generation. In *Advances in Neural Information Processing Systems (NeurIPS)*, 2022. 2
- [84] Jianjing Zhang, Hongyi Liu, Qing Chang, Lihui Wang, and Robert X Gao. Recurrent neural network for motion trajectory prediction in human-robot collaborative assembly. *CIRP annals*, 69(1):9–12, 2020. 1
- [85] Hongkai Zheng, Weili Nie, Arash Vahdat, Kamyar Azizzadenesheli, and Anima Anandkumar. Fast sampling of diffusion models via operator learning. In *International Conference on Machine Learning (ICML)*, 2023. 2
- [86] Mingyuan Zhou, Huangjie Zheng, Zhendong Wang, Mingzhang Yin, and Hai Huang. Score identity distillation: Exponentially fast distillation of pretrained diffusion models for one-step generation. In *Forty-first International Conference on Machine Learning*, 2024. 3

# MoFlow: One-Step Flow Matching for Human Trajectory Forecasting via Implicit Maximum Likelihood Estimation based Distillation

## Supplementary Material

The supplementary material is organized as follows. First, we introduce additional implementation details in Appendix A, including our MoFlow flow-matching objective in Appendix A.1, training and sampling steps in Appendix A.2 and Appendix A.3, as well as the architectural details in Appendix A.4. In Appendix B, we include additional qualitative results on the NBA sports dataset, demonstrating the effectiveness of our proposed methods. Moreover, we present additional ablation studies in Appendix C to showcase the success of inference-time speed-up, thanks to our IMLE distillation scheme in Appendix C.1, and the impact of training hyperparameters of IMLE in Appendix C.3.

### A. Further Implementation Details

#### A.1. Flow Matching Objective Formulation

In Sec. 4.2, we define the multi-modal motion prediction objective for the flow matching model and explain the key implementation details. To maintain self-consistency, we reintroduce the fundamental concepts from scratch.

Recall that our goal is to generate  $K$  trajectories  $\{Y_1, Y_2, \dots, Y_K\}$  to capture the diverse motion patterns of the agents under consideration, given their overall context information denoted as  $C$ . In the flow matching framework, we extend the notation by introducing a superscript to indicate flow time, with the denoising ODE intermediate states represented as  $\{Y_1^t, Y_2^t, \dots, Y_K^t\}, t \in [0, 1]$ .

However, in the dataset, we observe only a single future trajectory  $Y^1$  conditioned on the context  $C$ . This limitation prevents us from directly adopting the vanilla flow matching objective, which involves linearly mixing clean data and noisy vectors to construct training objectives. Instead, we utilize data-space prediction and develop the multi-modal learning loss accordingly.

To achieve this, we first transform the original loss, which involves learning a vector field  $v_\theta$ , into predicting the data at time  $t = 1$ :

$$\begin{aligned} \mathcal{L}_{\text{FM}} &= \mathbb{E}_{Y^t, Y^1, t} \left[ \left\| v_\theta(Y^t, C, t) - (Y^1 - Y^0) \right\|_2^2 \right], \\ &= \mathbb{E}_{Y^t, Y^1, t} \left[ \left\| v_\theta(Y^t, C, t) - \frac{Y^1 - Y^t}{1-t} \right\|_2^2 \right], \\ &= \mathbb{E}_{Y^t, Y^1, t} \left[ \left\| \frac{Y^t + (1-t)v_\theta(Y^t, C, t) - Y^1}{1-t} \right\|_2^2 \right]. \end{aligned}$$

We then define the network as a reparameterized model  $D_\theta$ , which implicitly learns the vector field  $v_\theta$  through a linear

transformation:

$$\begin{aligned} D_\theta(Y^t, C, t) &:= Y^t + (1-t)v_\theta(Y^t, C, t), \\ \mathcal{L}_{\text{FM}} &= \mathbb{E}_{Y^t, Y^1, t} \left[ \frac{\|D_\theta(Y^t, C, t) - Y^1\|_2^2}{(1-t)^2} \right]. \end{aligned}$$

Note that we are merely rearranging the network modules, while the loss functions remain exactly equivalent to those in the vanilla framework.

Next, we design a training loss to encourage the data prediction model  $D_\theta$  to learn multi-modal trajectories. To achieve this, we employ a standard Transformer structure (as illustrated in Fig. 1) to generate  $K$  correlated predictions. Specifically, the model  $D_\theta$  produces  $K$  scene-level waypoint predictions, denoted as  $\{S_i\}_{i=1}^K, S_i \in \mathbb{R}^{A \times 2T_f}$ , along with the corresponding classification logits  $\{\zeta_i\}_{i=1}^K, \zeta_i \in \mathbb{R}$ . For simplicity, we omit the time-dependent coefficients and apply a combined regression and classification loss as follows:

$$\bar{\mathcal{L}}_{\text{FM}} = \mathbb{E}_{Y^t, Y^1, t} \left[ \|S_{j^*} - Y^1\|_2^2 + \text{CE}(\zeta_{1:K}, j^*) \right], \quad (\text{A.1})$$

$$j^* = \arg \min_j \|S_j - Y^1\|_2^2, \quad (\text{A.2})$$

where  $\text{CE}(\cdot, \cdot)$  means the cross-entropy loss.

#### A.2. MoFlow Teacher Model Training

We present the training algorithm for the teacher model with a modified objective in Algorithm 2. Notably, we observe that using tied noise across all  $K$  components stabilizes the training process. In contrast, untied noise introduces excessive variability, making convergence significantly more challenging. For the flow time scheduler  $p_t(\cdot)$ , we employ a logit-normal distribution:  $\text{logit}(t) \sim \mathcal{N}(\mu_t, \sigma_t^2)$ . In practice, one can sample a random variable  $\kappa \sim \mathcal{N}(\mu_t, \sigma_t^2)$  and apply the standard logistic function,  $\frac{1}{1+e^{-\kappa}}$ , to obtain the desired samples for  $t$ . The parameters  $\mu_t = -0.5$  and  $\sigma_t = 1.5$  are selected based on a hyperparameter sweep.

Empirically, we observe that the data space prediction loss function defined in Eq. (A.1) suffers from overfitting when  $t$  is close to 1. This is because, in this regime, the noisy input  $Y_{1:K}^t$  becomes highly similar to the clean trajectory  $Y_{1:K}^1$ . When conditioned on the future trajectory  $Y_{1:K}^1$ , the noisy vector  $Y_{1:K}^t$  at time  $t$  follows a Gaussian distribution  $\mathcal{N}(tY_{1:K}^1, (1-t)^2I)$ . Its variance,  $(1-t)^2$ , decreases quadratically as  $t$  approaches 1. These overfitting effects cause the flow matching model to adopt a cheating solution during training, relying excessively on the input  $Y_{1:K}^t$

---

**Algorithm 2** MoFlow Teacher Model Training
 

---

- 1: **Require:** Training Dataset  $p_{\mathcal{D}}$ , learning rate  $\eta$ , teacher model  $D_{\theta}$  for data prediction
  - 2: Initialize the parameters  $\theta$  of the network  $D_{\theta}$ .
  - 3: **repeat**
  - 4:    $(Y^1, C) \sim p_{\mathcal{D}}$                     $\triangleright$  Sample observed data
  - 5:    $Y_s^0 \sim \mathcal{N}(\mathbf{0}, \mathbf{I})$
  - 6:    $Y_{1:K}^0 \leftarrow \text{repeat}(Y_s^0, K)$             $\triangleright$  Tied noise
  - 7:    $Y_{1:K}^1 \leftarrow \text{repeat}(Y^1, K)$
  - 8:    $t \sim p_t(t)$                             $\triangleright$  Time scheduler
  - 9:    $Y_{1:K}^t \leftarrow tY_{1:K}^1 + (1-t)Y_{1:K}^0$
  - 10:    $S_{1:K}, \zeta_{1:K} \leftarrow D_{\theta}(Y_{1:K}^t, C, t)$
  - 11:    $\theta \leftarrow \theta - \eta \nabla_{\theta} \mathcal{L}_{\text{FM}}(S_{1:K}, \zeta_{1:K}, Y^1)$     $\triangleright$  Eq. (A.1)
  - 12: **until** converged
- 

---

**Algorithm 3** MoFlow Teacher Model Sampling
 

---

- 1: **Require:** Evaluation dataset  $p'_{\mathcal{D}}$ , teacher model  $D_{\theta}$  for data prediction, sampling steps  $T$
  - 2: **repeat**
  - 3:    $(\cdot, C) \sim p'_{\mathcal{D}}$                             $\triangleright$  Sample context data
  - 4:    $Y_s^0 \sim \mathcal{N}(\mathbf{0}, \mathbf{I})$
  - 5:    $Y_{1:K}^0 \leftarrow \text{repeat}(Y_s^0, K)$             $\triangleright$  Tied noise
  - 6:   **for**  $n \in [0, 1, \dots, T-1]$  **do**
  - 7:      $S_{1:K}, \zeta_{1:K} \leftarrow D_{\theta}(Y_{1:K}^n, C, \tau_n)$
  - 8:      $v_{\theta}^{(i)} = \frac{S_i - Y_i^{\tau_n}}{1 - \tau_n}, \quad \forall i \in [K]$
  - 9:      $v_{\theta} = \text{concat}(v_{\theta}^{(1)}, v_{\theta}^{(2)}, \dots, v_{\theta}^{(K)})$
  - 10:     $Y_{1:K}^{\tau_{n+1}} \leftarrow Y_{1:K}^{\tau_n} + (\tau_{n+1} - \tau_n)v_{\theta}$
  - 11:   **end for**
  - 12: **until** finished
- 

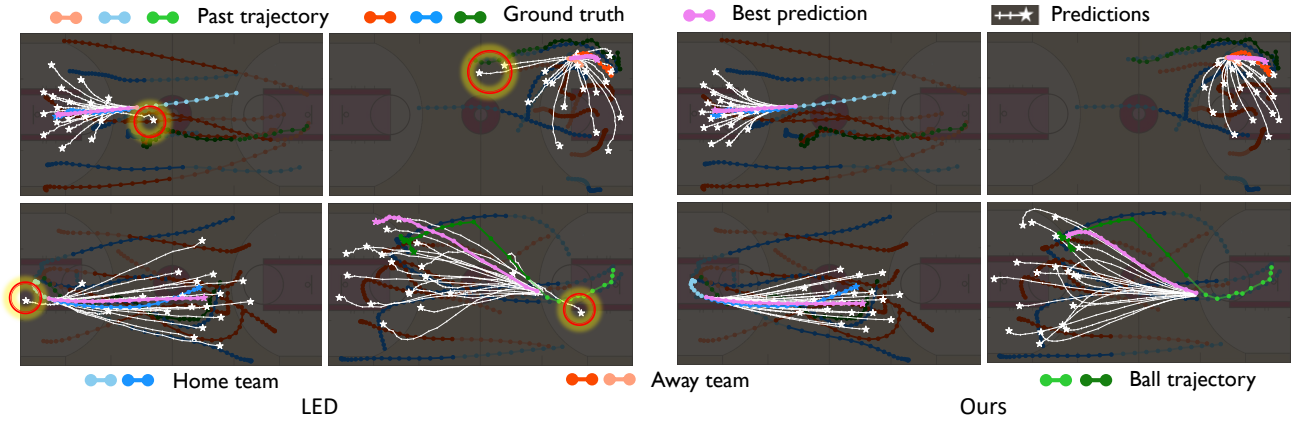


Figure 5. Qualitative results on NBA dataset in terms of diversity. Our method generates diverse samples that are more socially plausible. Some of the trajectories generated by LED model, which are highlighted by red circles, do not adhere to the basketball game patterns or rules. (Light color indicates past trajectory while dark color means future trajectory; blue/orange/green color: two teams and the basketball; pink color: the sample that is the closest to the Ground truth in  $L_2$  sense among  $K = 20$  predictions)

and generalizing poorly on the test dataset. To address this issue, we propose a flow time-dependent masking mechanism to encourage the model to extract useful signals from the context  $C$ . Specifically, we introduce a masking mechanism applied to the noise embedding, as illustrated in Fig. 1, which uses an S-shaped logistic function as the threshold:

$$f_m(t) = \frac{1}{1 + e^{-k(t-m)}}.$$

During training, for a randomly sampled time step  $t$  from the time scheduler, we mask the noisy embedding with zeros with a probability of  $f_m(t)$ . This serves as a simple embedding-level dropout mechanism, applied only during training. In our experiments, we set  $k = 20$  and  $m = 0.5$ .

### A.3. MoFlow Teacher Model Sampling

In Algorithm 3, we solve the denoising ODEs during sampling by leveraging the  $K$ -correlated trajectory predictions  $\{S_i\}_{i=1}^K$  produced by  $D_{\theta}$  to compute the  $K$ -shot vector

field:

$$v_{\theta}^{(i)} = \frac{S_i - Y_i^t}{1 - t}, \quad \forall i \in [K].$$

The initial values  $Y_i^0$  for all components are sampled from a standard normal distribution. The process iteratively updates  $Y_{1:K}^t$  based on the predicted vector field as the flow time  $t$  progresses towards  $t = 1$ .

We use a mapping function  $\tau_n$  to represent the actual flow time  $t$  at sampling iteration  $n \in [0, T]$ , given a total computation budget of  $T$  steps. The mapping function must satisfy two boundary conditions:  $\tau_0 = 0$  and  $\tau_T = 1$ . In our experiments, we set  $T = 100$ . Following [12, 51], we design a non-linear time mapping function as follows:

$$\tau_n = \begin{cases} \frac{n}{1000}, & \text{if } n \leq \frac{T}{2}, \\ \frac{T}{500} + \frac{(1.0 - \frac{T}{500})(n - \frac{T}{2})^p}{(\frac{T}{2})^p}, & \text{if } n > \frac{T}{2}. \end{cases}$$

Empirically, we set  $p = 5$  based on a hyperparameter grid search.

Table 5. Ablation study on various components of our MoFlow on the **NBA** dataset. (PE-K) Positional Encoding (PE) on number of predictions ( $K$ ); (PE-A) PE on agent-level only; (w/o PE) No PE; (Uniform) uniform noise/time schedule; (IID) i.i.d. noise instead of shared noise; (w/o Mask) Turn off the flow-time dependent masking mechanism; (Ours) Our MoFlow with all modules on. We report  $\min_{20}\text{ADE}/\min_{20}\text{FDE}$  (meters) for empirical performance. We **bold** the top results.

<i>Time</i>	PE-K	PE-A	w/o PE	Uniform	IID	w/o Mask	<b>Ours</b>
1.0s	<b>0.19</b> /0.26	0.41/0.74	0.45/0.84	<b>0.19</b> /0.26	0.26/0.44	<b>0.19</b> /0.27	<b>0.19/0.25</b>
2.0s	0.35/ <b>0.47</b>	0.88/1.77	1.02/2.10	0.35/0.48	0.59/1.12	0.38/0.56	<b>0.34/0.47</b>
3.0s	<b>0.52</b> /0.68	1.37/2.72	1.61/3.22	0.53/0.68	0.97/1.87	0.59/0.80	<b>0.52/0.67</b>
4.0s	<b>0.71</b> /0.88	1.83/3.51	2.14/4.05	<b>0.71</b> /0.88	1.36/2.46	0.82/1.07	<b>0.71/0.87</b>

#### A.4. Network Architecture

Building on prior studies [18, 45, 82], we adopt the spatio-temporal transformer encoder to jointly model temporal and social dimensions, capturing complex agent interactions over time and space. To enhance performance across datasets, the encoder architecture is dataset-specific: the spatio-temporal transformer encoder is used for ETH-UCY and SDD, while a PointNet-like encoder [52] is employed for the NBA dataset. Our spatio-temporal encoder processes both the context embedding and noise embedding through MLP layers, which are further combined with the flow-matching time signal during the teacher model’s training. The encoder for the student IMLE model employs a similar structure, differing only in its handling of the flow-matching time. In both transformer-based encoders leverage skip connections and share a configuration of 128 features, a feed-forward dimension of 512, eight attention heads, and consist of four layers.

In our the motion decoder, we employ additional self-attention to capture interactions among  $K$  scene predictions, as depicted in Fig. 1, complementing the temporal and social interactions modeled by the encoder. The embedding dimension, feed-forward dimension, and number of attention heads in the decoder match those of the spatial temporal encoder. The decoder comprises four blocks with each block performing factorized self-attention both over the sample dimension and the agent dimension [49]. To circumvent the potential overfitting issue, the attention dropout rate is set to 0.1.

Both our MoFlow model and the IMLE model are smaller in size compared to the LED initializer [45], with  $\sim 1\text{M}$  fewer parameters.

#### A.5. Model Training Details

We preprocess the trajectories using a simple min-max normalization technique, scaling future relative motion to the range  $[-1, 1]$  linearly to facilitate the training of the flow-matching model. A basic transformer architecture, depicted in Fig. 1, serves as the backbone of our approach. We find the standard transformer implementation to be sufficient for our task, requiring no special training tricks to

achieve strong performance. To facilitate the learning of inter-agent spatial relationships, we apply sinusoidal positional encoding across agents, assigning unique relative positions to each agent’s representation. In the motion decoder, we reinforce the agent-level positional encoding and introduce an additional positional encoding at the prediction level. Self-attention is then applied alternately at the agent and prediction levels, strengthening inter-agent interactions and improving overall scene coherence. The student model trained with IMLE objective shares the same architecture as the teacher model, except that it does not need the flow time positional encoding layers. For teacher model sampling, we adopt 100 steps to solve the denoising ODEs and generate samples. These samples are used both to evaluate teacher model performance and to train the IMLE distillation models. To enhance IMLE training efficiency, we compute and save the teacher model samples in advance. All the training is conducted on NVIDIA RTX6000 and A40 GPUs using the AdamW [38] optimizer in PyTorch [50], with weight decay set to 0.01.

## B. Further Qualitative Results

We would love to show more qualitative results on NBA dataset. In Fig. 5, we compare our 20 predictions with the samples<sup>3</sup> generated by LED [45] model. Upon closer examination of the predictions generated by the LED model, we observe that certain trajectories, which highlighted by the red circles, move in implausible, opposite directions. In contrast, our model effectively captures the general movement, steering the trajectories towards more plausible directions. Notably, the two figures in the first row of the LED model predictions are classified as backcourt violations defined in the basketball rules. Such violations are rare in the NBA training dataset. Notice that violations are not present in our predictions, indicating that our model generates trajectories that are more realistic and contextually appropriate for basketball games. There are additional comparisons

<sup>3</sup>Note that these are the exactly two same scenes with identical ego agents, as demonstrated by their paper and `codebase`. The coloring has been adjusted to align with our visualizations, and we have replaced their mean prediction with the best-of-20 prediction for consistency.



	$\omega = 0$				$\omega = 1$	$\omega = 5$
	DDPM	LED	MoFlow	IMLE	MoFlow*	MoFlow*
(a) @2s	0.44/0.64	0.37/0.57	<b>0.34/0.47</b>	<b>0.34/0.47</b>	0.37/0.52	0.42/0.61
(a) @4s	0.94/1.21	0.81/1.10	<b>0.71/0.87</b>	<b>0.71/0.86</b>	0.75/0.96	0.81/1.12
(b) @2s	1.15/2.30	0.89/1.84	<b>0.83/1.64</b>	<b>0.83/1.65</b>	0.84/1.68	0.86/1.73
(b) @4s	2.40/4.65	1.95/3.84	<b>1.71/3.34</b>	1.73/3.35	1.74/3.37	1.81/3.49
MASD [81]	6.41	15.74	5.85	5.78	5.54	5.00

Table 6. Joint metrics performance on NBA dataset. \* means we train our MoFlow using the new objective. (a)  $\min_{20} \text{ADE}/\min_{20} \text{FDE}$  metric; (b) a new metric  $\min_{20} \text{JADE}/\min_{20} \text{JFDE}$ ; (c) MASD diversity metric [62, 81]. DDPM refers to the stage-one diffusion model used in LED [45]. We use the checkpoint from the codebase provided by LED.

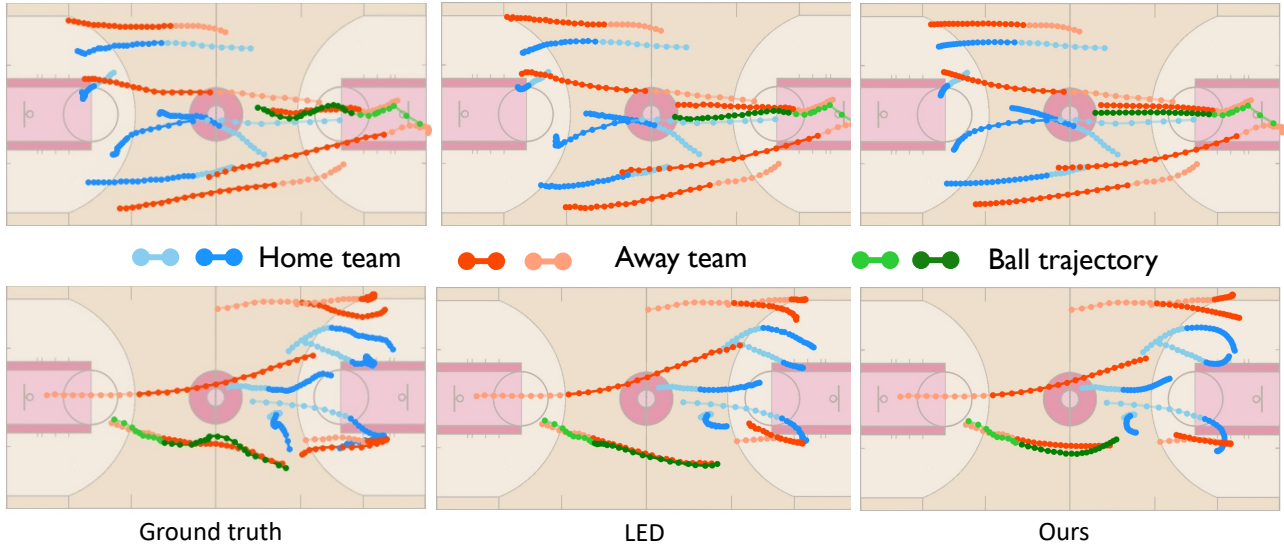


Figure 6. More qualitative results on the NBA dataset show a comparison between the best-of-20 predictions from our MoFlow IMLE distillation method, the best-of-20 predictions the LED method, and the ground truth future trajectories. The visualization demonstrates that our approach produces predictions that more closely align with the ground truth trajectories compared to the LED model. (Light color indicates past trajectory while dark color means future trajectory; blue/orange/green color: two teams and the basketball)

Table 7. Ablations on IMLE sample size  $m$  on the NBA dataset. We report  $\min_{20} \text{ADE}/\min_{20} \text{FDE}$  (meters) for performance.

Trajectory Time	$m = 5$	$m = 10$	$m = 20$	$m = 40$
1.0s	0.22/0.27	0.19/0.26	<b>0.18/0.25</b>	OOM
2.0s	0.38/0.42	<b>0.35/0.48</b>	<b>0.35/0.47</b>	OOM
3.0s	0.58/0.70	0.55/0.69	<b>0.52/0.67</b>	OOM
Total (4.0s)	0.78/0.95	0.73/0.89	<b>0.71/0.87</b>	OOM

on the trajectory diversity between LED and our model, as they follow the same patterns aforementioned in Fig. 9. According to Fig. 10, we have successfully predicted the direction of the future trajectories given the context on a regular basis while other state-of-the-art method failed to achieve. In particular, we highlight the subtle yet essential differences among the best-of-20 predictions from our MoFlow IMLE distillation method, the best-of-20 predictions from the LED method, and the ground truth future trajectories by zooming in on the details.

It is important to highlight that our MoFlow model can

generate  $K$  scene-level trajectory predictions, with corresponding classification logits  $\{\zeta_i\}_{i=1}^K, \zeta_i \in \mathbb{R}$ , depicted by Fig. 8 and Fig. 7. This means we have an empirical distribution for all the trajectories that we generate for each agent. While the predicted trajectories may sometimes be widely distributed, our MoFlow model effectively differentiates their plausibility.

## C. Additional Experimental Results

In this section, we conduct ablation experiments on the NBA dataset to validate our model design choices. Due to a recent paper [66], we will report another set of results under the joint metric to show the capacity of our models.

### C.1. Sampling Speed-up Effect

We demonstrate the sampling speed-up effect in Tab. 9, reporting the average sampling time per scene for runtime. Thanks to the one-step inference enabled by IMLE distillation, our student model achieves significantly faster sam-

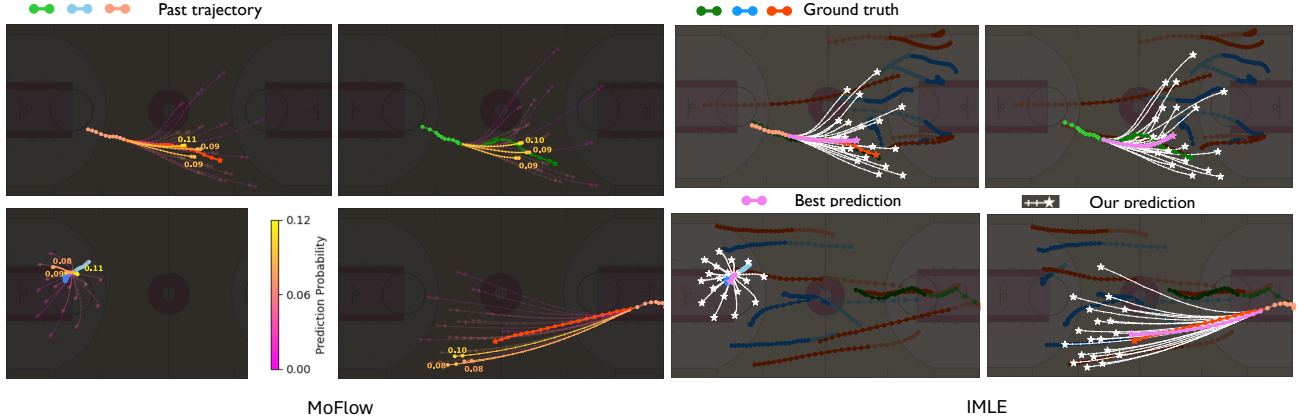


Figure 7. Some scenes from NBA dataset with MoFlow predictions for one agent and corresponding IMLE predictions.

Table 8. Comparison with baseline distillation models on **ETH-UCY** dataset.  $\min_{20}\text{ADE}/\min_{20}\text{FDE}$  (meters) are reported. Bold/underlined fonts represent the best/second-best result. Note that we evaluate our approach on this dataset with the same split as SGAN [19] while Tab. 2 is based on the dataset and train-test split released by the LED [45] group.

Subsets	MID [18]	GroupNet [73]	TUTR [56]	EqMotion [75]	EigenTraj [5]	LED [45]	SingularTraj [6]	MoFlow	IMLE
ETH	0.39/0.66	0.46/0.73	0.40/0.61	0.40/0.61	<u>0.36/0.53</u>	0.39/0.58	<b>0.35/0.42</b>	0.39/0.55	0.40/0.61
HOTEL	0.13/0.22	0.15/0.25	<b>0.11/0.18</b>	<u>0.12/0.18</u>	<u>0.12/0.19</u>	<b>0.11/0.17</b>	0.13/0.19	<b>0.11/0.17</b>	0.12/0.18
UNIV	<b>0.22/0.45</b>	0.26/0.49	<u>0.23/0.42</u>	<u>0.23/0.43</u>	0.24/0.34	0.26/0.44	0.25/0.44	<u>0.22/0.39</u>	0.24/0.44
ZARA1	0.17/0.30	0.21/0.39	0.18/0.34	0.18/ <u>0.32</u>	0.19/0.33	0.18/ <b>0.26</b>	0.19/0.32	<b>0.17/0.29</b>	<b>0.17/0.31</b>
ZARA2	<u>0.13/0.27</u>	0.17/0.33	<u>0.13/0.25</u>	<u>0.13/0.23</u>	0.14/0.24	<u>0.13/0.22</u>	0.15/0.25	<b>0.12/0.22</b>	0.13/0.24
AVG	<u>0.21/0.38</u>	0.25/0.44	<u>0.21/0.36</u>	0.32/0.35	<u>0.21/0.34</u>	<u>0.21/0.33</u>	<u>0.21/0.32</u>	<b>0.21/0.32</b>	0.21/0.36

pling with 100x fewer NFEs, reducing runtime by 98% on the same hardware. Notably, we found that IMLE distillation does not compromise empirical performance in our setup. Moreover, both our teacher and student model achieve faster sampling speeds than state-of-the-art methods, while delivering superior performance.

## C.2. Ablations on Flow Matching Configurations

To assess the significance of each module, we conduct an ablation study on different components of our MoFlow.

Table 9. Sampling speed-up comparison on the **NBA** dataset. We report  $\min_{20}\text{ADE}/\min_{20}\text{FDE}$  (meters) for empirical performance. DDPM refers to the teacher diffusion model used in LED [45].

Efficiency	MoFlow	IMLE	DDPM	LED
NFE	100	1	100	6
Runtime (ms)	33.20	0.70	796	22.38
Performance	MoFlow	IMLE	DDPM	LED
1.0s	0.18/0.25	0.18/0.25	0.20/0.28	0.18/0.27
2.0s	0.34/0.47	0.35/0.47	0.43/0.64	0.37/0.56
3.0s	0.52/0.67	0.52/0.67	0.68/0.95	0.58/0.84
Total (4.0s)	0.71/0.87	0.71/0.87	0.93/1.20	0.81/1.10

In Sec. 4.2, we discussed the design of input-output dimension adaptation and the time schedule. Here, we demonstrate the superiority of our current configuration through the results presented in Tab. 5.

From Tab. 5, we observe that positional encoding applied at the predictions ( $K$ ) level provides a greater advantage compared to positional encoding applied at the agent level. Additionally, incorporating shared noise yields strong final results without leading to the variance explosion observed in column (e).

## C.3. Ablations on IMLE Configurations

According to the IMLE training principle outlined in Algorithm 1, the student model needs to sample  $m > 1$  instances to select the one closest to the teacher model’s sample. We present the comparison results for different values of  $m$  in Tab. 7. We choose  $m = 20$  for its superior empirical performance. Note that  $m$  effectively enlarges the training-time mini-batch size by a factor of  $m$ . Therefore, setting  $m$  too large can lead to out-of-memory issues. Moreover, we present the JADE/JFDE results and conduct ablation on  $\omega$  in by re-training our MoFlow with the new objec-

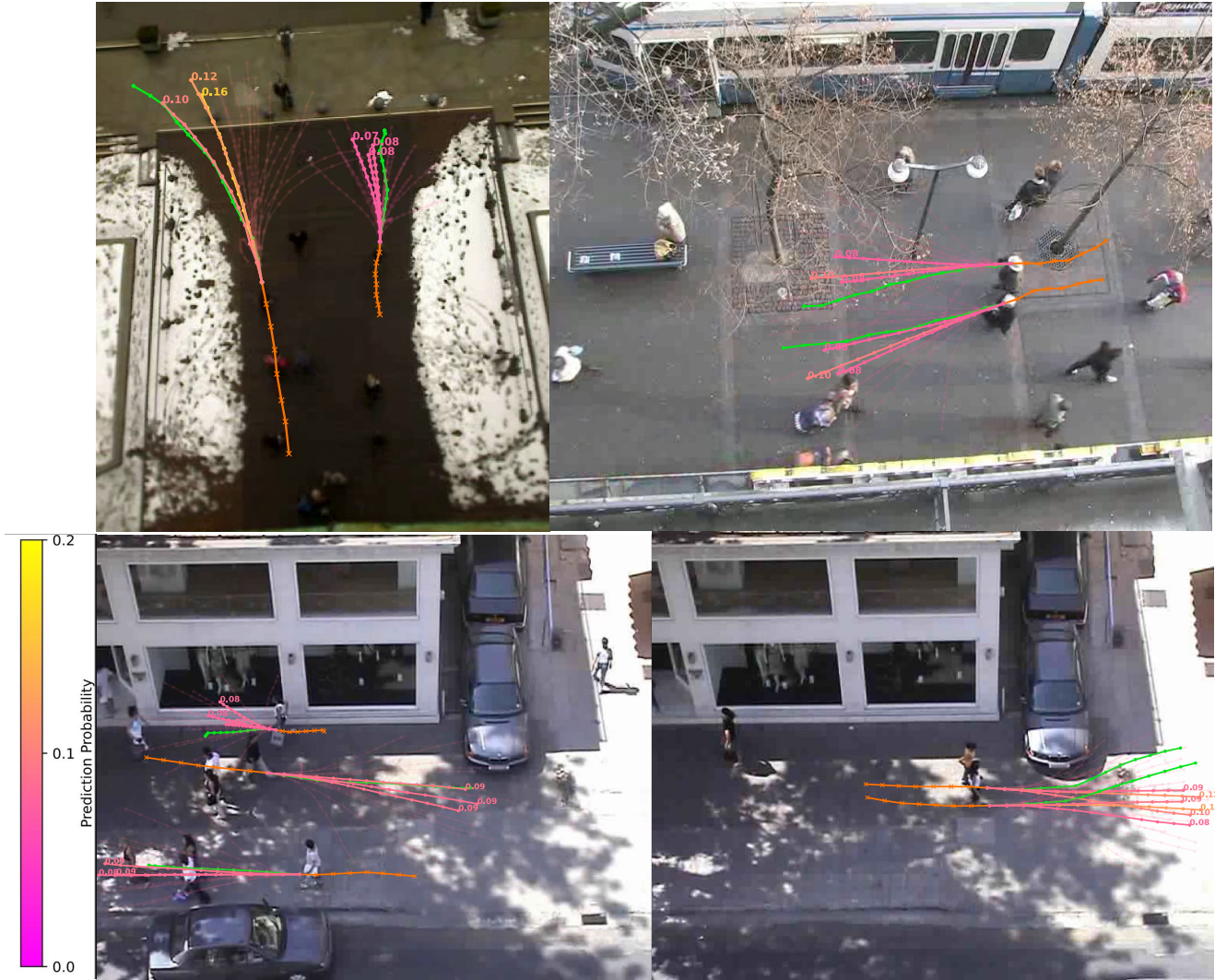


Figure 8. Scenes from ETH-UCY datasets with MoFlow generation. The probability besides the trajectories are normalized from classification logit  $\{\zeta_i\}_{i=1}^K$  via Softmax.

tive, which is identical to equations (10,11) [66]. Based on Tab. 6, we observe a trade-off between these two metrics: a marginal improvement in JADE/JFDE leads to a significant drop in ADE/FDE performance. Next, we assess our model’s ability to preserve the sample quality of the teacher model. Specifically, when analyzing the metric map-aware self-distance (MASD), we observe that the LED model fails to maintain this quantity, exhibiting a substantial deviation of  $\sim 9\text{m}$  from the teacher model (DDPM). In contrast, our IMLE model preserves this quantity with remarkable accuracy, achieving a deviation of only  $\sim 0.1\text{m}$ . These results further underscore the superiority of our approach in the distillation task.

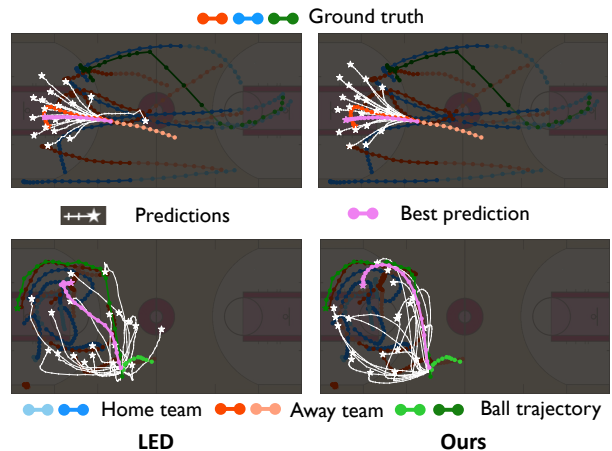


Figure 9. More qualitative results on NBA dataset in terms of diversity. We compare our model with LED again.

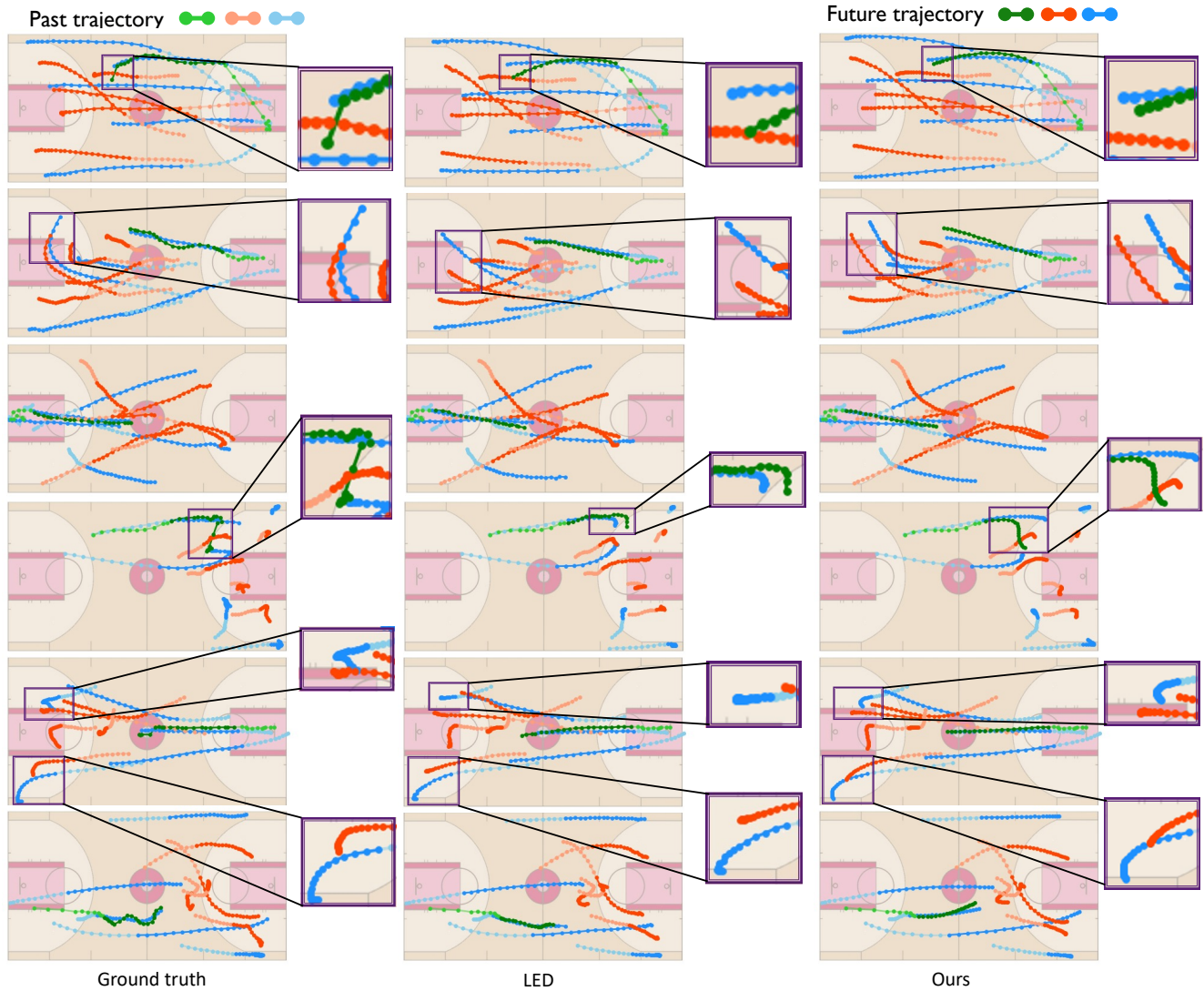


Figure 10. More qualitative results on the NBA dataset show a comparison among the best-of-20 predictions from our MoFlow IMLE distillation method, the best-of-20 predictions the LED method, and the ground truth future trajectories. The visualization demonstrates that our approach produces predictions that more closely align with the ground truth trajectories compared to the LED model. The key differences are zoomed in from the purple rectangles and displayed side-by-side, contrasting the ground truth, the best samples generated by the LED model with those produced by our approach. (blue/orange/green color: home team, away team and the basketball)